Satellite kinematics – III. Halo masses of central galaxies in SDSS

Surhud More,[1,2]*† Frank C. van den Bosch,[1,3] Marcello Cacciato,[1,4]‡
Ramin Skibba,[1,5] H. J. Mo and Xiaohu Yang[7]

[1]*Max Planck Institute for Astronomy, Koenigstuhl, 17, D69117 Heidelberg, Germany*
[2]*Kavli Institute for Cosmological Physics, University of Chicago, 933 East 56th Street, Chicago, IL 60637, USA*
[3]*Department of Physics and Astronomy, University of Utah, 115 South 1400 East, Salt Lake City, UT 84112-0830, USA*
[4]*Racah Institute of Physics, The Hebrew University, Jerusalem 91904, Israel*
[5]*Steward Observatory, University of Arizona, 933 N. Cherry Avenue, Tucson, AZ 85721, USA*
[6]*Department of Astronomy, University of Massachussets, Amherst, MA 010039305, USA*
[7]*Shanghai Astronomical Observatory, Nandan Road 80, Shanghai 200030, China*

ABSTRACT

We use the kinematics of satellite galaxies that orbit around the central galaxy in a dark matter halo to infer the scaling relations between halo mass and central galaxy properties. Using galaxies from the Sloan Digital Sky Survey, we investigate the halo mass–luminosity relation (MLR) and the halo mass–stellar mass relation (MSR) of central galaxies. In particular, we focus on the dependence of these scaling relations on the colour of the central galaxy. We find that red central galaxies on average occupy more massive haloes than blue central galaxies of the same luminosity. However, at fixed stellar mass there is no appreciable difference in the average halo mass of red and blue centrals, especially for $M_* \lesssim 10^{10.5}\,h^{-2}\,{\rm M_\odot}$. This indicates that stellar mass is a better indicator of halo mass than luminosity. Nevertheless, we find that the scatter in halo masses at fixed stellar mass is non-negligible for both red and blue centrals. It increases as a function of stellar mass for red centrals but shows a fairly constant behaviour for blue centrals. We compare the scaling relations obtained in this paper with results from other independent studies of satellite kinematics, with results from a SDSS galaxy group catalog, from galaxy–galaxy weak lensing measurements and from subhalo abundance matching studies. Overall, these different techniques yield MLRs and MSRs in fairly good agreement with each other (typically within a factor of 2), indicating that we are converging on an accurate and reliable description of the galaxy–dark matter connection. We briefly discuss some of the remaining discrepancies among the various methods.

Key words: methods: statistical – galaxies: haloes – galaxies: kinematics and dynamics – galaxies: structure – dark matter.

1 INTRODUCTION

The growth of structure in the Universe is predominantly driven by dark matter. The fluctuations in the dark matter density field grow under the action of gravity and form a web-like structure. Galaxies form as baryon condensates at the density peaks of this cosmic web. Understanding the connection between the distribution of galaxies and the underlying distribution of dark matter is crucial to understand the physics of galaxy formation. This galaxy–dark matter connection is often expressed in terms of the scaling relations

between the properties of galaxies and the mass of the dark matter halo in which they reside. Reliable measurements of the dark matter halo mass are essential to quantify these scaling relations. This can be accomplished with the help of numerous methods. These include techniques that are primarily used on individual systems such as rotation curves (e.g. Rubin et al. 1982), strong lensing of background galaxies (e.g. Gavazzi et al. 2007) and X-ray emission from hot gas in clusters (e.g. Dai, Kochanek & Morgan 2007; Rykoff et al. 2008). With the advent of large-scale galaxy redshift surveys, substantial progress has been made with methods that allow the inference of the dark matter halo masses in a statistical sense, e.g. the average halo mass as a function of various properties of galaxies. Such methods include the modelling of the clustering of galaxies (e.g. Yang, Mo & van den Bosch 2003; Zehavi et al. 2004; Collister & Lahav 2005; Tinker et al. 2005; Zehavi et al. 2005; Skibba et al.

2006; van den Bosch et al. 2007; Brown et al. 2008; Skibba & Sheth 2009), galaxy–galaxy weak lensing (e.g. Seljak 2000; McKay et al. 2001; Mandelbaum et al. 2006; Parker et al. 2007; Mandelbaum, Seljak & Hirata 2008; Schulz, Mandelbaum & Padmanabhan 2009) and a combination of the two (e.g. Yoo et al. 2006; Cacciato et al. 2009; Li et al. 2009).

The satellite galaxies that orbit within the dark matter haloes of their central galaxies are also excellent probes of the dark matter halo mass. Their kinematics reflect the depth of the dark matter potential well they orbit. The number of satellites in massive systems like clusters is large enough to obtain a reliable measure of their kinematics and hence the halo mass (e.g. Carlberg et al. 1996; Carlberg, Yee & Ellingson 1997). However, in low-mass systems, where only a handful of satellites can be detected per central, one has to adopt a stacking procedure to quantify the kinematics of satellites (Erickson, Gottesman & Hunter 1987; Zaritsky et al. 1993; Zaritsky & White 1994; Zaritsky et al. 1997). Central galaxies with similar properties (e.g. luminosity) are stacked together and the velocity information of their satellites is combined to obtain a quantitative measure of the kinematics of the satellites. Various studies of the kinematics of satellite galaxies have now been carried out using large redshift surveys to improve the sample size of satellites (McKay et al. 2002; Brainerd & Specian 2003; Prada et al. 2003; Conroy et al. 2005; Becker et al. 2007; Conroy et al. 2007; Norberg, Frenk & Cole 2008). The sample sizes in these studies have been limited by their use of strict isolation criteria to identify centrals and satellites, specifically designed to avoid misidentifications. van den Bosch et al. (2004) devised relaxed selection criteria which were iteratively adapted to the luminosity of central galaxies to circumvent this problem. Their criteria improved the sample size by nearly an order of magnitude over studies that use strict isolation criteria while still maintaining low levels of contamination. The improved statistics have warranted a better study of the systematics and selection effects that bias the kinematic measurements (Norberg et al. 2008).

In More, van den Bosch & Cacciato (2009b, hereafter Paper I), we showed that if the relation between the halo mass and the stacking property has a non-negligible scatter then the kinematics of the satellites of the stacked system can be difficult to interpret. This issue has been neglected by most previous studies. We presented a new method to infer both the average halo mass and the scatter in halo masses as a function of the property used to stack the central galaxies. In More et al. (2009a, hereafter Paper II), this method was applied to galaxies from the Sloan Digital Sky Survey (SDSS) (York et al. 2000) to infer the halo mass–luminosity relation of central galaxies (hereafter MLR). It was found that both the average and the scatter of the MLR of central galaxies increase with the luminosity of the central galaxy.

The scatter in the MLR is an interesting quantity, as it is related to the stochasticity in galaxy formation. Two important, related questions are: (i) what is the physical origin of this stochasticity, and (ii) what galaxy property is most closely related to the mass of the halo in which it resides (i.e. shows the least amount of scatter at a given halo mass). The answer to (i) yields valuable insight into the physics of galaxy formation, while the answer to (ii) identifies the optimal galaxy property to trace the cosmic density field. It is well known that galaxies of the same stellar mass may have very different luminosities, even after correction for dust extinction. Galaxies with younger stellar populations will typically be bluer and more luminous than galaxies of the same stellar mass, but with an older stellar population. It may well be that the stellar mass of a central galaxy is a better indicator of halo mass than its luminosity,

in which case the halo mass–stellar mass relation of central galaxies (hereafter MSR) will have less scatter than the MLR, and the scatter in the MLR will be correlated with the colour of the central galaxy. Obviously, since we lack a complete theory of galaxy formation, it may also be that the opposite holds, and that the scatter in the MLR is actually less than that in the MSR. In this paper, we investigate these issue by measuring the kinematics of satellite galaxies as functions of both the luminosity and stellar mass of centrals split by colour into red and blue subsamples. Using the methodology outlined in Paper I, we use these to probe both the means and scatters of the MLR and MSR of red and blue galaxies.

This paper is organized as follows. In Section 2, we describe the data used in this paper. In Section 3, we explain our method of analysis. In particular, we describe the procedure used to identify the centrals and the satellites, the measurement of the kinematics of satellites and the subsequent modelling to determine the halo masses of central galaxies. In Section 4 we present our results and compare them with other independent studies. Finally, we summarize our findings in Section 5.

Throughout this paper we adopt the cosmological parameters supported by the 7-yr data release of *WMAP* (Komatsu et al. 2010); $\Omega_{\rm m} = 0.266$, $\Omega_{\Lambda} = 0.734$, $h = H_0/100\,{\rm km\,s^{-1}\,Mpc^{-1}} = 0.71$, the spectral index of initial density fluctuations $n_{\rm s} = 0.963$ and the normalization of the power spectrum of density fluctuations $\sigma_8 = 0.809$. We use the symbol M to refer to the mass of a dark matter halo, which is defined as the mass enclosed within a spherical overdensity $\delta\rho/\bar{\rho} = 200$, where $\bar{\rho}$ denotes the mean matter density of the universe.

2 DATA

We use data from the SDSS which is a joint five-passband (u, g, r, i and z) imaging and medium-resolution ($R \sim 1800$) spectroscopic survey (York et al. 2000). More specifically, we use the New York University Value Added Galaxy Catalogue (Blanton et al. 2005), which is based upon SDSS Data Release 4 (Adelman-McCarthy et al. 2006) but includes a set of significant improvements over the original pipelines. The magnitudes and colours of the galaxies are based upon the standard SDSS Petrosian technique and have been k-corrected and evolution corrected to $z = 0.1$ using the method described in Blanton et al. (2003a,b). The notations $^{0.1}(g - r)$ and $^{0.1}M_r - 5\log h$ are used to denote the resulting $(g - r)$ colour and the absolute magnitude of the galaxies. From this catalogue, we select all galaxies in the main galaxy sample with apparent magnitudes less than 17.77 that lie in an area where the redshift completeness limit of the survey $\mathcal{C} > 0.8$. Next we construct a volume-limited sample that is complete in luminosity above a $^{0.1}r$-band luminosity of $L_{\rm min} = 10^{9.5}\,h^{-2}\,{\rm L_\odot}$.[1] The redshift range that we adopt for this volume-limited sample is $0.02 \le z \le 0.071$, which results in a total sample of 55 415 galaxies.

Stellar masses are indicated by M_* and are computed using the relation between the stellar mass-to-light ratio and the $^{0.0}(g - r)$ colour provided by Bell et al. (2003):

$$\log\left[\frac{M_*}{h^{-2}\,{\rm M_\odot}}\right] = -0.306 + 1.097\,[^{0.0}(g - r)] - 0.10$$
$$- 0.4\,(^{0.0}M_r - 5\log h - 4.64). \quad (1)$$

---

[1] The $^{0.1}r$-band magnitude of the Sun in the AB system equal to 4.76 (Blanton et al. 2003a) is used to convert the absolute magnitude of a galaxy to its luminosity in units of $h^{-2}\,{\rm L_\odot}$.

Here $^{0.0}(g-r)$ and $^{0.0}M_r - 5\log h$ denote the $(g-r)$ colour and the r-band absolute magnitude of galaxies k-corrected and evolution corrected to $z = 0.0$, 4.64 is the r-band magnitude of the Sun in the AB system, and the -0.10 term is a result of adopting the Kroupa (2001) initial mass function (see Borch et al. 2006). The typical uncertainties in the stellar masses obtained in this manner are of the order of ∼0.1 dex (Bell et al. 2003).

We classify galaxies to be red or blue based upon their bimodal distribution in the $^{0.0}(g-r)$ colour–stellar mass plane (Baldry et al. 2004). We use the following separation criterion to demarcate the boundary between red and blue galaxies in the colour–stellar mass plane (see Appendix A):

$$^{0.0}(g-r)_{\text{cut}} = 0.65 + 0.10\left\{\log\left[M_*/(h^{-2}\,\text{M}_\odot)\right] - 10.0\right\}. \quad (2)$$

3 METHODOLOGY

3.1 Selection criteria

The first step towards measuring the kinematics of satellite galaxies in the SDSS is to accurately identify central galaxies and their associated satellites. For our analysis of the MLR we proceed as follows. A galaxy is identified to be a central if it is brighter than every other galaxy within a cylindrical volume specified by $R < R_{\text{h}}$ and $|\Delta V| < (\Delta V)_{\text{h}}$ centred on itself. Here R is the physical distance from the galaxy under consideration projected on the sky and ΔV is the line-of-sight (hereafter los) velocity difference between two galaxies. All galaxies that lie within a cylindrical volume specified by $R < R_{\text{s}}$ and $|\Delta V| < (\Delta V)_{\text{s}}$ around a central galaxy, and that are fainter than the central galaxy, are labelled to be its satellites. The criteria used to select the sample of central and satellite galaxies for the analysis of the MSR are almost identical, except that in this case the central galaxy must have the largest stellar mass in its cylindrical volume specified by R_{h} and $(\Delta V)_{\text{h}}$.

The parameters R_{h}, $(\Delta V)_{\text{h}}$, R_{s} and $(\Delta V)_{\text{s}}$ define the sizes of the cylinders used to identify central galaxies and their satellites. Contrary to most previous studies of satellite kinematics (McKay et al. 2002; Brainerd & Specian 2003; Prada et al. 2003; Conroy et al. 2005, 2007; Norberg et al. 2008), we do not use fixed values for these parameters. Rather, since halo mass is expected to be positively correlated with the luminosity or stellar mass of the central galaxies, we scale the selection parameters according to the property of the galaxy under consideration. Following van den Bosch et al. (2004), we adopt $R_{\text{h}} = 0.8\sigma_{200}\,h^{-1}$ Mpc, $(\Delta V)_{\text{h}} = 1000\sigma_{200}$ km s^{-1}, $R_{\text{s}} = 0.15\sigma_{200}\,h^{-1}$ Mpc and $(\Delta V)_{\text{s}} = 4000$ km s^{-1}. Here σ_{200} is the satellite velocity dispersion in units of 200 km s^{-1}, which we parametrize as

$$\sigma_{200}(\log Q_{10}) = a + b(\log Q_{10}) + c(\log Q_{10})^2, \quad (3)$$

where Q_{10} is either the central galaxy luminosity in units of $10^{10}\,h^{-2}\,\text{L}_\odot$ or the stellar mass in units of $10^{10}\,h^{-2}\,\text{M}_\odot$, depending upon the property used to stack central galaxies. Clearly, since the determination of σ_{200} requires a sample of centrals and satellites, this selection method has to be iterative. Fixed values of the selection criteria parameters are used to identify the central and the satellite galaxies in the first iteration. The velocity dispersion of the selected satellites as a function of the central galaxy property, parametrized via equation (3), is fit using a maximum likelihood method and subsequently used to scale the values of the parameters that define the selection criteria. These are used to select a new sample of centrals and satellites, and the entire procedure is

Table 1. Selection criteria parameters.

Samples	a	b	c	Centrals	Satellites
LA	2.19	0.38	0.32	3755	5953
LR	2.23	0.38	0.29	2602	4682
LB	2.11	0.46	−0.16	997	1151
SA	2.07	0.22	0.21	3675	6004
SR	2.11	0.19	0.20	2963	5230
SB	1.98	0.48	−0.17	751	666

The parameters *a*, *b* and *c* that define the criteria used to select central and satellite galaxies for all the samples used in this paper (see text), and the total numbers of centrals and satellites thus selected.

repeated until convergence.[2] Using detailed mock galaxy redshift surveys, van den Bosch et al. (2004) have shown that this iterative technique yields much lower interloper fractions than the more common method using fixed cylindrical volumes (see also Paper II). For completeness, and to allow the reader to reproduce our results, Table 1 lists the final iteration criteria used for our various samples (in terms of the parameters *a*, *b* and *c* that appear in equation 3), as well as the total number of centrals and satellites selected in each sample. Note that these parameters differ depending on the centrals we choose to stack for our analysis. The sample of centrals and satellites selected when the selection criteria are tuned based on the velocity dispersion around all centrals stacked by luminosity (stellar mass) is called Sample LA (SA). Samples LR (SR) and LB (SB) are selected by tuning the selection criteria parameters based upon the velocity dispersion around red and blue centrals stacked by luminosity (stellar mass), respectively.

3.2 Velocity dispersion measurement

In Paper I we demonstrated that the commonly measured velocity dispersion of satellite galaxies, σ_{sat}, cannot be used to uniquely determine the scaling relation between halo mass and a central galaxy property *unless this relation has zero scatter*. In fact, we have shown that different scaling relations with different amounts of scatter can yield exactly the same σ_{sat}. In the same paper, however, we have shown that this degeneracy can be broken using a combination of two different measures for the velocity dispersion of the satellite galaxies: satellite-weighted (σ_{sw}^2) and host-weighted (σ_{hw}^2). To measure the velocity dispersion in these two different schemes, the satellite galaxies in the final sample are first binned into subsamples based upon the properties (luminosity or stellar mass) of their central galaxies. For each bin, the distribution of los velocities of satellite galaxies with respect to their centrals, $P(\Delta V)$, is constructed by either giving each satellite equal weight (satellite-weighting) or a weight equal to $1/N_{\text{sat}}$ (host-weighting), where N_{sat} denotes the number of satellites around the host of the satellite under consideration. As shown in Paper I, the difference between σ_{sw}^2 and σ_{hw}^2 depends on the amount of scatter in the scaling relation between halo mass and central galaxy property,[3] and allows the degeneracy to be broken.

In order to extract the satellite velocity dispersion (satellite-weighted or host-weighted) from the corresponding $P(\Delta V)$ distributions, we fit $P(\Delta V)$ using the sum of two Gaussians plus a

---

[2] We refer the reader to Paper II and van den Bosch et al. (2004) for details regarding this method.
[3] In the case of zero scatter, one has that $\sigma_{\text{sw}} = \sigma_{\text{hw}}$.

constant:

$$P(\Delta V) = a_0 + a_1 \exp\left[\frac{-(\Delta V^2)}{2\sigma_1^2}\right] + a_2 \exp\left[\frac{-(\Delta V^2)}{2\sigma_2^2}\right]. \qquad (4)$$

The satellite velocity dispersion (satellite-weighted or host-weighted) then follows from

$$\sigma_{(\text{sw/hw})}^2 = \left[\frac{a_1\sigma_1^3 + a_2\sigma_2^3}{a_1\sigma_1 + a_2\sigma_2}\right] - \sigma_{\text{err}}^2. \qquad (5)$$

Here σ_{err} is the contribution to the effective variance of $P(\Delta V)$ due to redshift errors in the SDSS. Given that each individual galaxy has a redshift error of $\sim 35\,\text{km}\,\text{s}^{-1}$, the error on the velocity difference, ΔV, of the central and satellite galaxies is $\sigma_{\text{err}} = \sqrt{2} \times 35 \simeq 49.5\,\text{km}\,\text{s}^{-1}$, which is the value we adopt throughout. The error bars on the velocity dispersions were estimated as the variance in the velocity dispersions obtained by fitting 1000 realizations of the $P(\Delta V)$ histogram (generated assuming Poisson error bars) with the procedure described above. Detailed tests using mock catalogues have shown that the above method yields extremely reliable estimates of the actual velocity dispersions (see Paper II).

Applying this method to the central-satellite samples selected using the criteria described in Section 3.1, we obtained the satellite-weighted and host-weighted velocity dispersions as well as the average number of satellites per central as a function of luminosity for samples LA, LR and LB, and as a function of stellar mass for samples SA, SR and SB. In addition, we also measured the fraction of red central galaxies as a function of luminosity from Sample LA and as a function of stellar mass from Sample SA. In the following subsection we describe how to use these data to constrain the MLR and MSR of central galaxies.

3.3 The model

The satellite-weighted and host-weighted velocity dispersions of satellites and the average number of satellites of a central galaxy with a given property depend on the distribution of halo masses of central galaxies with that property, $P(M|Q)$. Therefore these observables can be used to infer the mean and the scatter of the scaling relation between halo mass and the central galaxy property. The analytical expressions that describe these three quantities are given by (see Paper I):

$$\sigma_{\text{sw}}^2(Q) = \frac{\int_0^\infty P(M|Q)\,\langle N_{\text{s}}\rangle_{\text{ap},M}\,\left\langle\sigma_{\text{sat}}^2\right\rangle_{\text{ap},M}\,\mathrm{d}M}{\int_0^\infty P(M|Q)\,\langle N_{\text{s}}\rangle_{\text{ap},M}\,\mathrm{d}M}, \qquad (6)$$

$$\sigma_{\text{hw}}^2(Q) = \frac{\int_0^\infty P(M|Q)\,\mathcal{P}(M)\,\left\langle\sigma_{\text{sat}}^2\right\rangle_{\text{ap},M}\,\mathrm{d}M}{\int_0^\infty P(M|Q)\,\mathcal{P}(M)\,\mathrm{d}M}, \qquad (7)$$

$$\langle N_{\text{s}}\rangle(Q) = \frac{\int_0^\infty P(M|Q)\langle N_{\text{s}}\rangle_{\text{ap},M}\mathrm{d}M}{\int_0^\infty P(M|Q)\mathcal{P}(M)\mathrm{d}M}. \qquad (8)$$

Here $\langle N_{\text{s}}\rangle_{\text{ap},M}$ and $\langle\sigma_{\text{sat}}^2\rangle_{\text{ap},M}$ denote the average number of satellites and the average velocity dispersion of satellites within the aperture R_{s} in a halo of mass M, respectively. The factor $\mathcal{P}(M)$ is the fraction of haloes of mass M that host at least one satellite. Our way of modelling the observables thus consists of two parts: (i) the kinematics of satellite galaxies in a single halo of a given mass and (ii) the statistics that describe how central and satellite galaxies occupy haloes. We describe each of these parts in the following subsections.

3.3.1 Kinematics in a single halo

We assume that dark matter haloes are spherically symmetric and that their density distributions follow the universal NFW profile (Navarro, Frenk & White 1997),

$$\rho(r|M) \propto \left(\frac{r}{r_{\text{s}}}\right)^{-1}\left(1 + \frac{r}{r_{\text{s}}}\right)^{-2}, \qquad (9)$$

where r_{s} is a scale radius specified in terms of the virial radius r_{vir} using the concentration parameter, $c = r_{\text{vir}}/r_{\text{s}}$. We use the concentration–mass relation from Macciò et al. (2007), appropriately modified for our definition of the halo mass. We assume that the number density distribution of satellite galaxies, $n_{\text{sat}}(r|M)$, is given by

$$n_{\text{sat}}(r|M) \propto \left(\frac{r}{\mathcal{R}r_{\text{s}}}\right)^{-\gamma}\left(1 + \frac{r}{\mathcal{R}r_{\text{s}}}\right)^{\gamma-3}. \qquad (10)$$

Here γ represents the slope of the number density distribution of satellites as $r \to 0$ and $\mathcal{R}$ is a free parameter. Throughout this paper, we use the result from Paper II that the number density distribution of satellites in the SDSS can be well described by equation (10) with $\gamma = 0.0$ and $\mathcal{R} = 2$ (see also Yang et al. 2005 and More 2009c). The distribution $n_{\text{sat}}(r|M)$ is normalized such that

$$\langle N_{\text{s}}\rangle(M) = 4\pi \int_0^{r_{\text{vir}}} n_{\text{sat}}(r|M)\,r^2\,\mathrm{d}r, \qquad (11)$$

where $\langle N_{\text{s}}\rangle(M)$ denotes the average number of satellites in a halo of mass M. The number of satellites within the aperture, $\langle N_{\text{s}}\rangle_{\text{ap},M}$, is then given by

$$\langle N_{\text{s}}\rangle_{\text{ap},M} = 4\pi \int_0^{R_{\text{s}}} R\,\mathrm{d}R \int_R^{r_{\text{vir}}} n_{\text{sat}}(r|M)\,\frac{r\,\mathrm{d}r}{\sqrt{r^2 - R^2}}. \qquad (12)$$

We further assume that the satellite occupation numbers follow Poisson statistics, which is supported both by direct observations (e.g. Yang, Mo & van den Bosch 2008) and by numerical simulations (Kravtsov et al. 2004). The fraction of central galaxies that have at least one satellite within the aperture radius R_{s} is then given by

$$\mathcal{P}(M) = 1 - \exp[-\langle N_{\text{s}}\rangle_{\text{ap},M}]. \qquad (13)$$

To find an analytical expression for $\langle\sigma_{\text{sat}}^2\rangle_{\text{ap},M}$, first note that the Jeans equation can be used to find an expression for the radial velocity dispersion of satellites at a radial distance r from the centre:

$$\sigma_{\text{sat}}^2(r|M) = \frac{c\,V_{\text{vir}}^2}{\mathcal{R}^2\mu(c)}\left(\frac{r}{\mathcal{R}r_{\text{s}}}\right)^\gamma\left(1 + \frac{r}{\mathcal{R}r_{\text{s}}}\right)^{3-\gamma}$$
$$\times \int_{r/r_{\text{s}}}^\infty \frac{\mu(x)\mathrm{d}x}{(x/\mathcal{R})^{\gamma+2}(1 + x/\mathcal{R})^{3-\gamma}}. \qquad (14)$$

Here V_{vir} is the circular velocity at r_{vir} and

$$\mu(x) = \int_0^x y(1+y)^{-2}\mathrm{d}y, \qquad (15)$$

(see Paper I for a detailed derivation). If the velocity dispersion of the satellites is assumed to be isotropic, then $\langle\sigma_{\text{sat}}^2\rangle_{\text{ap},M}$ can be expressed as the average of the radial velocity dispersion, $\sigma_{\text{sat}}^2(r|M)$, over the aperture R_{s}:

$$\left\langle\sigma_{\text{sat}}^2\right\rangle_{\text{ap},M} = \frac{4\pi}{\langle N_{\text{s}}\rangle_{\text{ap},M}} \int_0^{R_{\text{s}}} R\,\mathrm{d}R$$
$$\times \int_R^{r_{\text{vir}}} n_{\text{sat}}(r|M)\,\sigma_{\text{sat}}^2(r|M)\,\frac{r\,\mathrm{d}r}{\sqrt{r^2 - R^2}}. \qquad (16)$$

We note that in order to derive the aperture averaged velocity dispersion in a halo of given mass, we made two key assumptions:

(i) the dark matter halo is spherically symmetric and, (ii) the orbits of the satellites are isotropic. The first assumption is justified because we are modelling the velocity dispersion of satellites that were obtained by stacking central galaxies without regard to their orientation. This to first order, erases out effects of non-sphericity in the potential of haloes. The effects of anisotropic orbits were studied analytically by van den Bosch et al. (2004). It was found that although the anisotropy in the orbits of satellite galaxies can affect the radial velocity dispersion profiles, the aperture-averaged velocity dispersions, like the ones we use, are more robust against biases introduced by anisotropic orbits.

3.3.2 Halo occupation statistics

To model the kinematics of satellite galaxies around central galaxies stacked by a particular property, we need to specify the distribution of halo masses for central galaxies with that property, $P(M|Q)$. Let us first consider the case of central galaxies stacked by luminosity and colour. In this case, $Q \equiv L \cap C$, where L denotes the luminosity of the central galaxy and C its colour. We will use the letters R for red and B for blue when referring to the actual colours. Using Bayes' theorem,

$$P(M|L \cap C) = \frac{P(L|M \cap C)\, f_C(M)\, P(M)}{f_C(L)\, P(L)}. \quad (17)$$

Here $P(L|M \cap C)$ describes the distribution of central galaxy luminosities in haloes of mass M that host central galaxies of a particular colour C, $f_C(M) = P(C|M)$ is the fraction of haloes of mass M that host a central galaxy of colour C and $P(M)$ is proportional to the halo mass function $n(M)$.[4] Note that the denominator has no dependence on M and is just a multiplicative normalization constant which cancels out when we model our observables (see equations 6–8).

We use simple parametric forms to model the distribution $P(L|M \cap C)$ and $f_C(M)$. The distribution $P(L|M \cap C)$ is assumed to be a lognormal given by

$$P(L|M \cap C) = \frac{\log(e)}{\sqrt{2\pi}\sigma_{\log L}} \exp\left[-\frac{(\log[L/\tilde{L}])^2}{2\sigma_{\log L}^2} \right] \frac{dL}{L}. \quad (18)$$

Here $\log \tilde{L}(C, M)$ denotes the mean of the lognormal distribution and $\sigma_{\log L}(C)$ is the corresponding scatter. We use four parameters each to specify the relations $\tilde{L}(R, M)$ and $\tilde{L}(B, M)$: a low-mass end slope, γ_1; a high-mass end slope, γ_2; a characteristic mass scale, M_1; and a normalization, L_0:

$$\tilde{L} = L_0 \frac{(M/M_1)^{\gamma_1}}{[1 + (M/M_1)]^{\gamma_1 - \gamma_2}}. \quad (19)$$

We further assume that the scatters $\sigma_{\log L}(R)$ and $\sigma_{\log L}(B)$ are independent of halo mass. Thus for each colour C, we use five parameters to describe the distribution $P(L|M \cap C)$. This parametrization is motivated by the results of Yang et al. (2008), who inferred the conditional luminosity function using the large SDSS galaxy group catalogue of Yang et al. (2007).

The function $f_R(M)$ is assumed to be linear in $\log M$:

$$f_R'(M) = f_0 + \alpha_f [\log(M/h^{-1}M_\odot) - 12.0],$$
$$f_R(M) = \min\{\max[0, f_R'(M)], 1.0\}, \quad (20)$$

---

[4] For the analysis in this paper, we use the halo mass function of Tinker et al. (2008) for which haloes are defined as spheres with an average density that is 200 times the average matter density in the universe.

where the second equality takes into account that f_R is a fraction, and therefore bounded by zero and unity (cf. van den Bosch et al. 2003). Also note that $f_B(M) = 1 - f_R(M)$, as 'red' and 'blue' form a mutually exclusive and exhaustive set of colours assigned to the central galaxies. Hence, $f_R(M)$ and $f_B(M)$ add a total of two free parameters to our model.

We also need a model for the satellite occupation numbers, $\langle N_s \rangle(M)$. Throughout we assume that the number of satellite galaxies in a halo of mass M scales with halo mass as

$$\langle N_s \rangle(M) = N_{12} \left(\frac{M}{10^{12}\, h^{-1}M_\odot} \right)^\alpha, \quad (21)$$

which adds two more parameters to our model; N_{12} and α. We experimented by setting $\langle N_s \rangle(M)$ to zero when it falls below N_{cut} to mimic an exponential cut-off in $\langle N_s \rangle(M)$ at small halo masses, with values of N_{cut} ranging from 0.001 to 0.1 and found that it does not significantly affect our results. Also note that we assume that $\langle N_s \rangle(M)$ is independent of the colour of the central galaxies. Although we believe this to be a realistic assumption, we will discuss the potential impact of its violations in Section 4.

Next, consider the case where galaxies are stacked only according to their luminosity, i.e. $Q \equiv L$. To model the observables we need to know the distribution

$$P(M|L) = \frac{P(L|M)\, P(M)}{P(L)} \propto P(L|M)\, n(M). \quad (22)$$

The distribution $P(L|M)$ is related to the distributions $P(L \cap R|M)$ and $P(L \cap B|M)$ according to

$$P(L|M) = P(L|M \cap R) f_R(M) + P(L|M \cap B) f_B(M). \quad (23)$$

Finally, the expression that describes the fraction of red centrals as a function of central galaxy luminosity is given by

$$f_R(L) = \frac{\int_0^\infty P(L|M \cap R)\, \mathcal{P}(M)\, n(M)\, f_R(M) dM}{\int_0^\infty P(L|M)\, \mathcal{P}(M)\, n(M) dM}. \quad (24)$$

Note that we have appropriately corrected for the fact that the observed fraction of red centrals is calculated using only those centrals that have at least one satellite.

Hence, our analytical model has a total of 14 free parameters and completely describes the kinematics of satellite galaxies and the average number of satellites around centrals stacked by luminosity in Samples LA, LR and LB. This analytical framework also allows us to calculate the fraction of red centrals as a function of luminosity.

For the analysis of the kinematics of satellite galaxies around centrals stacked by stellar mass, there is an additional complication that has to be addressed. The central and satellite galaxies used for our analysis are selected from a volume-limited sample that is complete above a certain luminosity. Since we have used both colour and luminosity to assign the stellar masses, our sample starts to become incomplete in stellar mass roughly below $10^{10}\, h^{-2}\, M_\odot$. The completeness is a function of both stellar mass and colour, and is described by the sample selection function $S(M_*, C)$, defined as the fraction of galaxies of stellar mass M_* and colour C in the SDSS volume with $0.02 \leq z \leq 0.071$ (i.e. our sample volume) that make it into the sample. The determination of $S(M_*, C)$ is discussed in Appendix A.

The sample selection function $S(M_*, C)$ enters our model in the following way. We can write the stacking property as $Q \equiv M_* \cap C \cap \hat{S}$, where we use $\hat{S}$ to denote the subset of all galaxies with stellar mass M_* and colour C in our sample volume that make it into the sample. The corresponding distribution of halo masses,

$P(M|M_* \cap C \cap \hat{S})$, can then be written as

$$P(M|M_* \cap C \cap \hat{S}) = \frac{P(\hat{S}|M \cap M_* \cap C)\, P(M \cap M_* \cap C)}{P(M_* \cap C \cap \hat{S})}$$

$$= \frac{S(M_*, C)}{P(M_* \cap C \cap \hat{S})}\, f_C(M)\, P(M)\, P(M_*|M \cap C). \tag{25}$$

In the second equality, we have identified the distribution $P(\hat{S}|M \cap M_* \cap C)$ as the selection function, $S(M_*, C)$. In addition, we have also expressed $P(M \cap M_* \cap C)$ in terms of $P(M_*|M \cap C)$. Note that the selection function does not depend on the halo mass M and acts as a multiplicative normalization constant for the distribution $P(M|M_* \cap C \cap \hat{S})$. It harmlessly cancels out from the expressions that analytically describe the observables when central galaxies are stacked by colour. However, it turns out to be important for calculating $P(M|M_* \cap \hat{S})$ and hence the observables when central galaxies are stacked by stellar mass alone. First note that the distribution $P(M|M_* \cap \hat{S})$ is related to $P(M_*|M \cap \hat{S})$ such that

$$P(M|M_* \cap \hat{S}) = \frac{P(M_* \cap \hat{S}|M)\, P(M)}{P(M_* \cap \hat{S})}. \tag{26}$$

The distribution $P(M_* \cap \hat{S}|M)$ can be expressed in terms of $P(M_*|M \cap R)$ and $P(M_*|M \cap B)$ as follows:

$$P(M_* \cap \hat{S}|M) = P(M_* \cap R \cap \hat{S}|M) + P(M_* \cap B \cap \hat{S}|M)$$

$$= f_R(M)\, S(M_*, R)\, P(M_*|M \cap R)$$

$$+ f_B(M)\, S(M_*, B)\, P(M_*|M \cap B). \tag{27}$$

Similar to equation (18), we parametrize $P(M_*|M \cap C)$ as a log-normal distribution with mean $\log \tilde{M}_*(C, M)$ and a scatter $\sigma_{\log M_*}$ which depends on colour but is independent of halo mass. The relation $\tilde{M}_*(C, M)$ is described using equation (19), but with L replaced by M_*, and we assume that the scatters $\sigma_{\log M_*}(R)$ and $\sigma_{\log M_*}(B)$ are independent of halo mass. For $f_R(M)$ and $\langle N_s \rangle(M)$ we adopt the same parametrizations as before (i.e. equations 20 and 21). Hence, our model for the analysis of the MSR also contains 14 free parameters, which we constrain using the observables obtained by stacking central galaxies by stellar mass and colour.

3.4 Constraining the model parameters

We now describe our method to constrain the model parameters. Here we focus on the analysis of the MLR, but note that the analysis of the MSR is basically the same. We have measurements of the satellite-weighted velocity dispersion, the host-weighted velocity dispersion and the average number of satellites per central, for 10 different luminosity bins, and for each of the three samples LA, LR and LB. In addition, we have 10 measurements of the fraction of red centrals as a function of luminosity. Since most of the centrals in sample LA are present in either sample LR or sample LB, the velocity dispersions and average number of satellites measured from sample LA are not independent of those obtained using samples LR and LB. Therefore, we do not use these measurements from sample LA to constrain the model parameters. This leaves a total of 70 independent data points to constrain our 14 model parameters.

We use flat uninformative priors on each of the model parameters (albeit in a limited interval for each of the parameters). We use a Monte Carlo Markov chain (hereafter MCMC) technique to sample from the posterior probability distribution of each of these parameters given the observational constraints. The MCMC is a chain of models, each consisting of the 14 parameters. At any point in the chain, a trial model is generated with the 14 free parameters

drawn from a 14-dimensional Gaussian proposal distribution which is centred on the current values of the parameters. The chi-squared statistic, χ^2_{try}, for this trial model, is calculated using

$$\chi^2_{\text{try}} = \sum_{C=R,B} \left[\chi^2_{\text{sw}}(C) + \chi^2_{\text{hw}}(C) + \chi^2_{\text{ns}}(C) \right] + \chi^2_{\text{fr}}, \tag{28}$$

where

$$\chi^2_{\text{sw}}(C) = \sum_{i=1}^{10} \left[\frac{\sigma_{\text{sw}}(Q[i]) - \hat{\sigma}_{\text{sw}}(Q[i])}{\Delta \hat{\sigma}_{\text{sw}}(Q[i])} \right]^2, \tag{29}$$

$$\chi^2_{\text{hw}}(C) = \sum_{i=1}^{10} \left[\frac{\sigma_{\text{hw}}(Q[i]) - \hat{\sigma}_{\text{hw}}(Q[i])}{\Delta \hat{\sigma}_{\text{hw}}(Q[i])} \right]^2, \tag{30}$$

$$\chi^2_{\text{ns}}(C) = \sum_{i=1}^{10} \left[\frac{\langle N_s \rangle(Q[i]) - \hat{N}_s(Q[i])}{\Delta \hat{N}_s(Q[i])} \right]^2, \tag{31}$$

$$\chi^2_{\text{fr}} = \sum_{i=1}^{10} \left[\frac{f_R(L) - \hat{f}_R(L[i])}{\Delta \hat{f}_R(L[i])} \right]^2. \tag{32}$$

Here $Q \equiv L \cap C$, $\hat{X}$ denotes the observable X and $\Delta \hat{X}$ its corresponding error. The trial step is accepted with a probability given by

$$P_{\text{accept}} = \begin{cases} 1.0, & \text{if } \chi^2_{\text{try}} \leq \chi^2_{\text{cur}} \\ \exp\left[-(\chi^2_{\text{try}} - \chi^2_{\text{cur}})/2\right], & \text{if } \chi^2_{\text{try}} > \chi^2_{\text{cur}}, \end{cases} \tag{33}$$

where χ^2_{cur} denotes the χ^2 for the current model in the chain.

We initialize the chain from a random position in our 14-dimensional parameter space and discard the first 20 000 models (the 'burn-in' period) allowing the chain to sample from a more probable part of the distribution. We proceed and construct a chain consisting of 40 million models. We thin this chain by a factor of 10^3 to remove the correlations between neighbouring models. This leaves us with a chain of 40 000 independent models that sample the posterior distribution. We use this chain of models to estimate the confidence levels on the parameters and the relations of interest, namely the mean and the scatter of the scaling relation between halo mass and the central galaxy property under consideration.

## 4 RESULTS

4.1 The halo mass–luminosity relation

The analysis of the MLR of central galaxies is carried out by analyzing Samples LA, LR and LB (see Table 1 for the selection criteria and the numbers of centrals and satellites in each of these samples). The host-weighted velocity dispersion, the satellite-weighted velocity dispersion and the average number of satellites as a function of the luminosity of the central galaxies obtained from Samples LR are shown as open squares in panels (a), (b) and (c) of Fig. 1, respectively. In the same figure, panels (d), (e) and (f) show the corresponding observables obtained from Sample LB. At fixed luminosity, the velocity dispersion of satellite galaxies around red centrals are systematically larger than the velocity dispersions around blue centrals. The same is also true for the average number of satellites. The fraction of red centrals as a function of luminosity obtained from Sample LA are shown in panel (g). The data in these seven panels are used to constrain the 14 parameters of our model that describe the halo occupation statistics of red and blue centrals, and
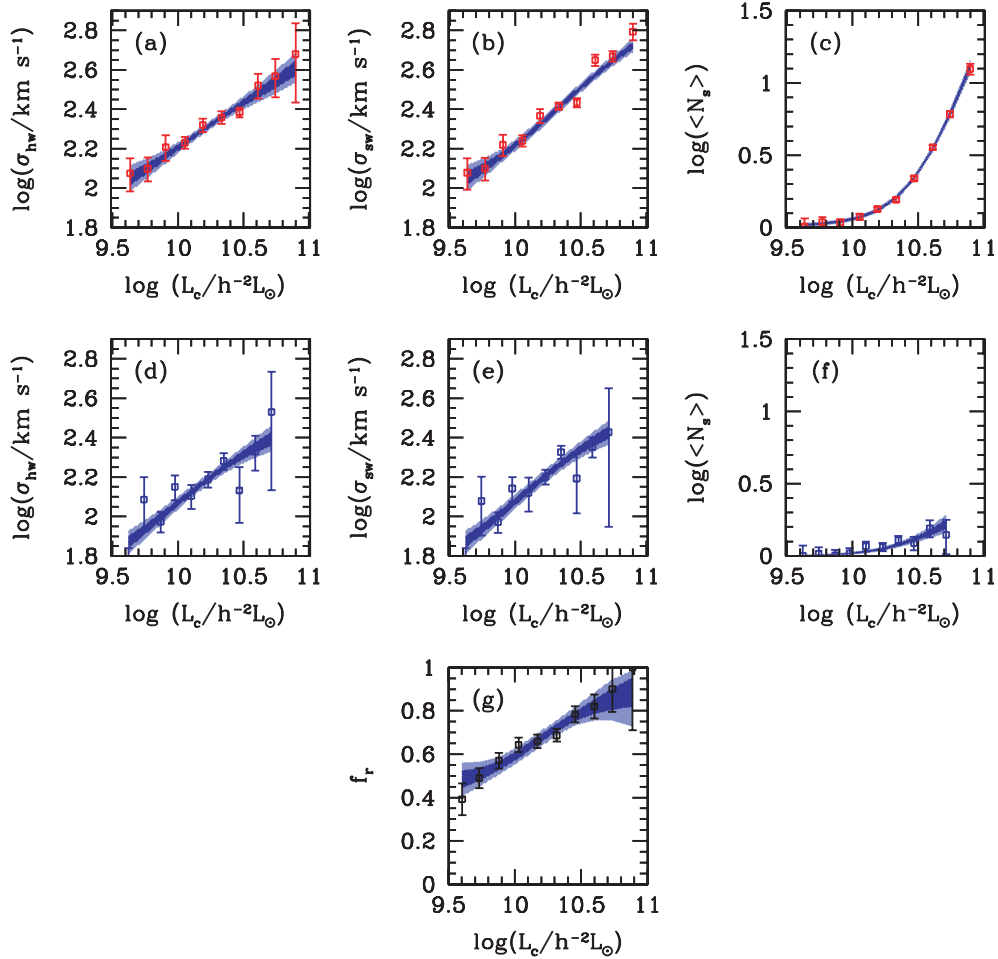
Figure 1. Observables used to constrain the MLR of central galaxies (open squares with error bars). The upper and middle panels show the observables measured using red centrals (Sample LR) and blue centrals (Sample LB), respectively. From the left to the right these panels show the host-weighted velocity dispersions [panels (a) and (d)], the satellite-weighted velocity dispersions [panels (b) and (e)] and the average number of satellites per central [panels (c) and (f)], all as a function of the luminosity of the central. Panel (g) shows the fraction of red centrals as a function of luminosity as measured from Sample LA. The dark and the faint blue regions indicate the 68 and 95 per cent confidence intervals obtained from the MCMC, showing that the model accurately fits the data.

the satellite occupation numbers in haloes that host red and blue centrals. The dark and faint blue shaded regions indicate the 68 and 95 per cent confidence levels obtained from our MCMC. A comparison with the data reveals that the model accurately reproduces the data.

Fig. 2 shows the velocity dispersions and the average number of satellites as a function of luminosity around *all* centrals obtained from Sample LA. As for samples LR and LB, the model is in excellent agreement with the data (open squares), even though these data were not directly used to constrain the model.
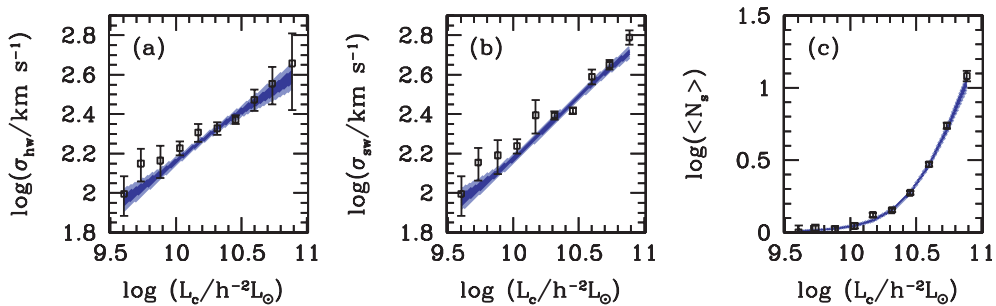
Figure 2. Observables measured using Sample LA. Panels (a), (b) and (c) shows the host-weighted velocity dispersions, the satellite-weighted velocity dispersions and the average number of satellites per central, respectively, all as a function of the luminosity of the central galaxy. Although these observables are not used to constrain the model parameters (see text), the 68 and 95 per cent confidence intervals obtained from the MCMC, indicated by the dark and faint blue regions, show that the model accurately fits these data as well.

Table 2. MLR: percentiles of the posterior distributions.

	Parameter	16 per cent	50 per cent	84 per cent	Best fit
Red centrals	$\log(L_0)$	9.63	9.86	10.17	9.99
	$\log(M_1)$	11.14	11.47	11.83	11.50
	γ_1	2.45	3.43	4.49	4.88
	γ_2	0.28	0.36	0.42	0.31
	$\sigma_{\log L}$	0.18	0.21	0.23	0.20
Blue centrals	$\log(L_0)$	9.08	9.36	9.64	9.55
	$\log(M_1)$	10.09	10.32	10.68	10.55
	γ_1	2.27	3.02	4.18	2.13
	γ_2	0.30	0.41	0.52	0.34
	$\sigma_{\log L}$	0.15	0.21	0.26	0.24
All centrals	f_0	0.59	0.65	0.71	0.70
	α_f	0.14	0.20	0.25	0.15
	$\log N_{12}$	−0.92	−0.81	−0.70	−0.78
	α	1.20	1.29	1.39	1.28

The 16, 50 and 84 percentile values of the posterior distributions for the parameters and the best-fitting parameters of our model obtained from the MCMC analysis of the velocity dispersion data from Samples LR, LB and LA. The best-fitting model has a reduced $\chi^2 = 0.88$.

The 16, 50 and 84 percentile values of the posterior distribution for our model parameters obtained from our analysis are listed in Table 2. The constraints on our model ingredients are presented pictorially in Fig. 3. Panels (a) and (d) show the constraints obtained on $\log \tilde{L}(M)$ for red and blue centrals, respectively, while panels (b) and (e) show the corresponding posterior distributions of the scatter in luminosities at fixed halo masses. Panel (c) shows the average number of satellite galaxies as a function of halo mass, and panel (f) shows the fraction of red centrals as a function of halo mass. At the bright end, the mean luminosity of red central galaxies scales with halo mass as $L \propto M^{0.36^{+0.06}_{-0.08}}$ while that of blue central galaxies

scales as $L \propto M^{0.41^{+0.11}_{-0.11}}$. At the faint end, the constraints on the faint-end slope of the $\log \tilde{L}(M)$ relation are entirely dominated by the prior $\gamma_1 \in [2.0, 5.0]$. This is due to the magnitude limit of the SDSS, which is not sufficiently faint to reliably probe the occupation statistics of dark matter haloes with $M \lesssim 10^{12} h^{-1} \, M_\odot$ (but see Yang, Mo & van den Bosch 2009). For the scatter in $P(L|M)$ we obtain that $\sigma_{\log L} = 0.21^{+0.02}_{-0.03}$ for red centrals and $\sigma_{\log L} = 0.21^{+0.05}_{-0.06}$ for blue centrals. Note that the scatter for blue centrals is less well constrained than for red centrals, which is due to the smaller sample size (see Table 1).

The slope of the relation $\langle N_s \rangle (M)$ that we obtain is $\alpha = 1.29 \pm 0.10$. We admit that the slope we obtain is on the higher side than what is found in the literature (Zehavi et al. 2005; Zheng, Coil & Zehavi 2007; Yang, Mo & van den Bosch 2008), but it is consistent with the slopes obtained by these studies within 3σ. We have experimented by assuming priors on the value of α from the results of Yang et al. (2008). In this case, the data still seem to prefer larger values of α and the fits get worse.

Fig. 4 shows the average halo mass and the scatter in halo masses obtained from our analysis for red centrals (left-hand panels), blue centrals (middle panels) and all centrals (right-hand panels) as a function of luminosity. As expected, brighter galaxies reside on average in more massive haloes. Note that the scatter in halo masses around all centrals appears somewhat higher than that around either red or blue centrals. This indicates that some fraction of this scatter is due to the fact that red and blue centrals of the same luminosity reside, on average, in haloes of different mass (see below). However, red and blue centrals separately still reveal a significant amount of scatter in their halo masses, whereby the scatter around red centrals increases with luminosity, while that around blue centrals shows no clear luminosity dependence.

The left-hand panel of Fig. 5 summarizes these results. It compares the MLR of red centrals (triangles) to that of blue centrals (circles) and to that of all centrals (squares). At fixed luminosity,
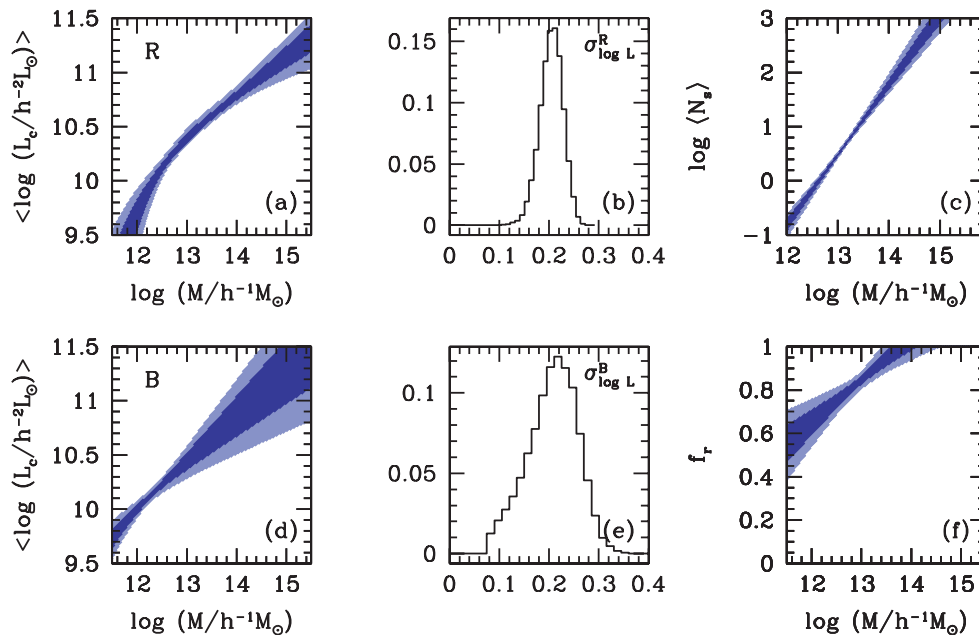

Figure 3. Constraints on the model ingredients obtained from the MCMC. The 68 and 95 per cent confidence intervals are indicated as dark and faint blue regions, respectively. Panel (a) shows the average luminosity of red centrals as a function of halo mass, while panel (b) shows the posterior distribution of the scatter $\sigma_{\log L}$ in this relation. Panels (d) and (e) show the same but for blue centrals. Panel (c) shows the constraints on the average number of satellites as a function of halo mass, and finally, panel (f) shows the constraints on the fraction of red centrals as a function of halo mass.
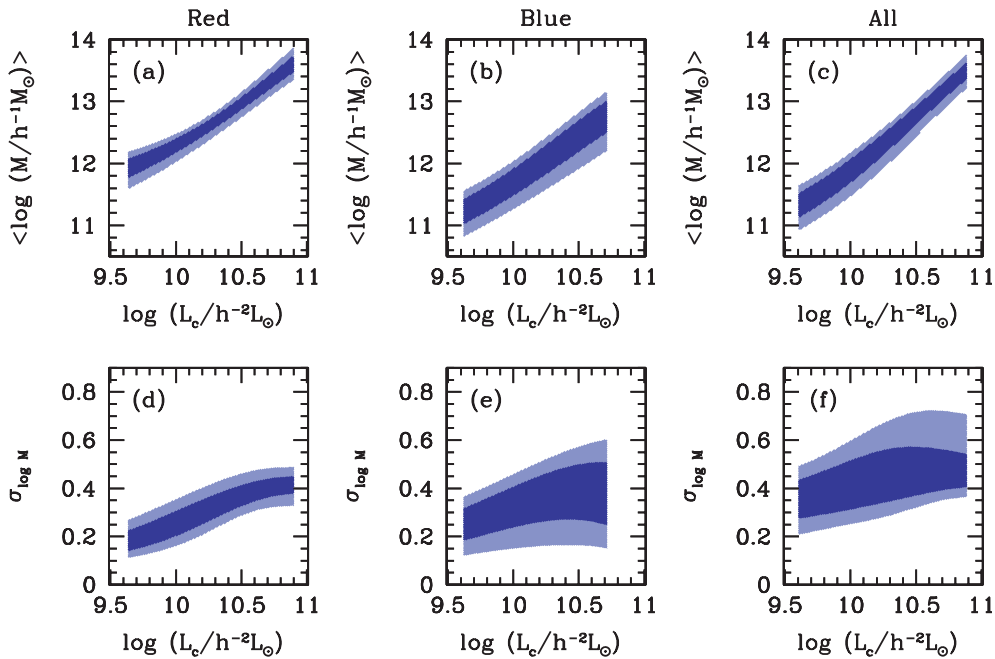
Figure 4. Constraints on the MLR obtained from the MCMC. The average halo masses as a function of the luminosity of red centrals, blue centrals and all centrals are shown in panels (a), (b) and (c), respectively. Panels (d), (e) and (f) show the confidence intervals on the scatter in these relations. As in the previous figures, dark and faint blue colours indicate the 68 and 95 per cent confidence intervals.
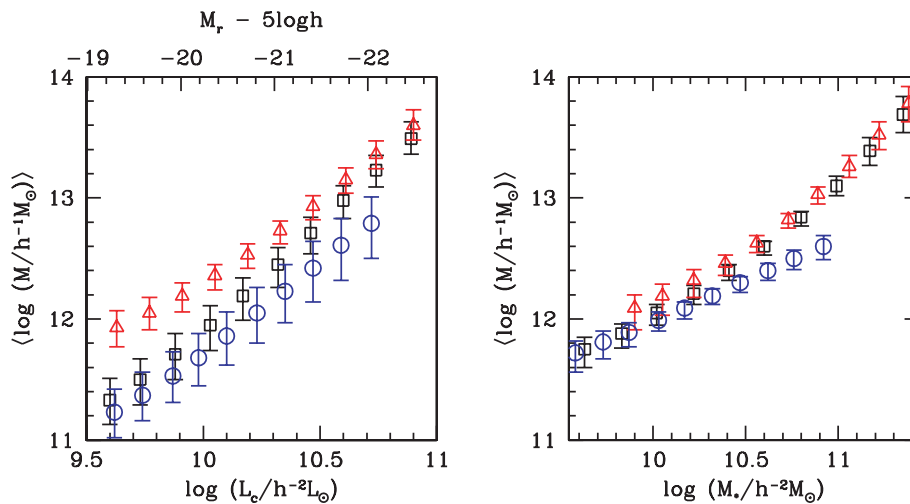

Figure 5. Comparison between the average MLR (left-hand panel) and the average MSR (right-hand panel) of all centrals (squares), red centrals (triangles) and blue centrals (circles). Error bars indicate the 68 per cent confidence intervals. See text for discussion.

red centrals on average reside in more massive haloes than blue centrals. As expected, the MLR of all centrals lies in between that of red and blue centrals. As the fraction of red centrals steadily increases to unity at the bright end, the average halo mass of all centrals shifts from tracing the MLR of blue centrals to tracing the MLR of red centrals.

4.2 The halo mass–stellar mass relation

The analysis of the MSR of central galaxies is carried out by analysing Samples SA, SR and SB (see Table 1 for the selection criteria and the numbers of centrals and satellites in each of these samples). The host-weighted velocity dispersion, the satellite-weighted velocity dispersion and the average number of satellites as

a function of the stellar mass of the central galaxies obtained from Samples SR are shown as open squares in panels (a), (b) and (c) of Fig. 6, respectively. In the same figure, panels (d), (e) and (f) show the corresponding observables obtained from Sample SB. At fixed stellar mass, the velocity dispersion of satellite galaxies around red centrals is systematically larger than that around blue centrals. The same is also true for the average number of satellites. The fraction of red centrals as a function of stellar mass obtained from Sample SA is shown in panel (g). The sharp drop of f_r to zero at the low stellar mass end is due to our use of a volume-limited sample complete in luminosity, which causes the sample selection function for red centrals to go to zero at the low-mass end (see Appendix A). The data in these seven panels are used to constrain the 14 parameters of our model. The dark and faint blue shaded regions indicate the 68
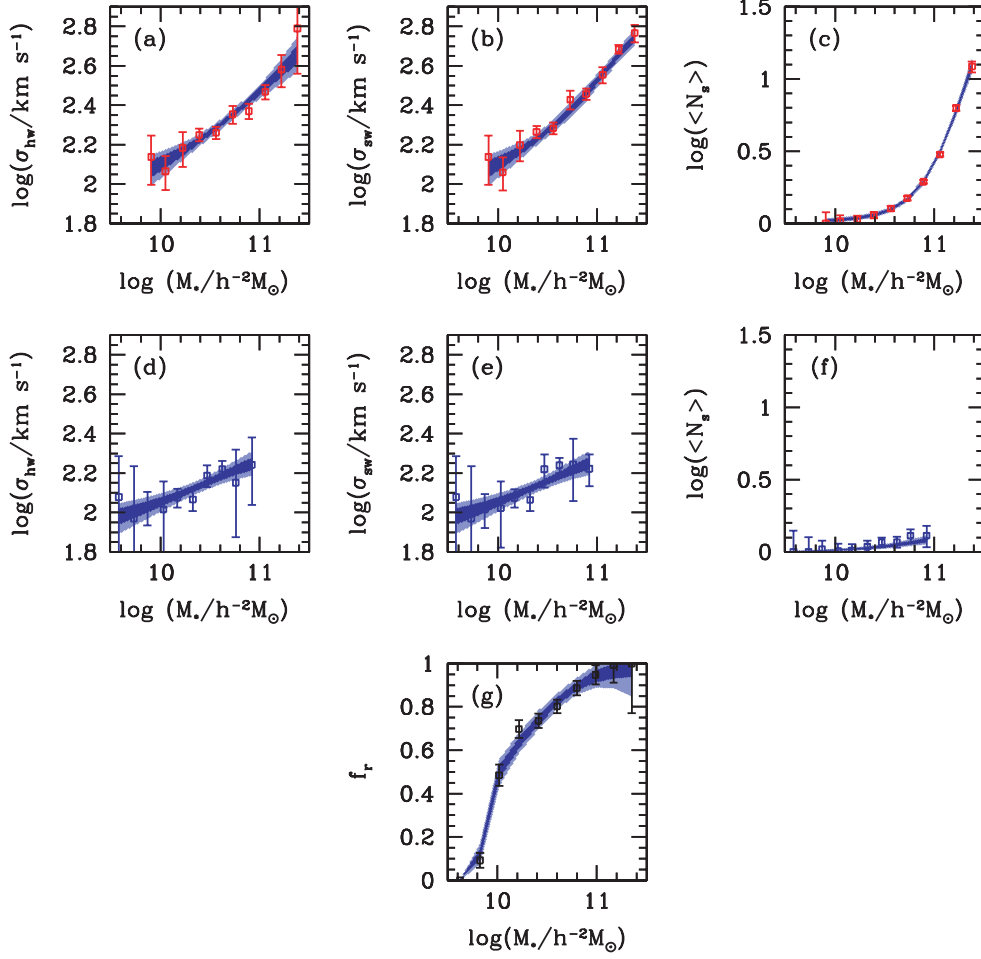
Figure 6. Same as Fig. 1, but as a function of the stellar mass of the centrals, based on samples SR, SB and SA.
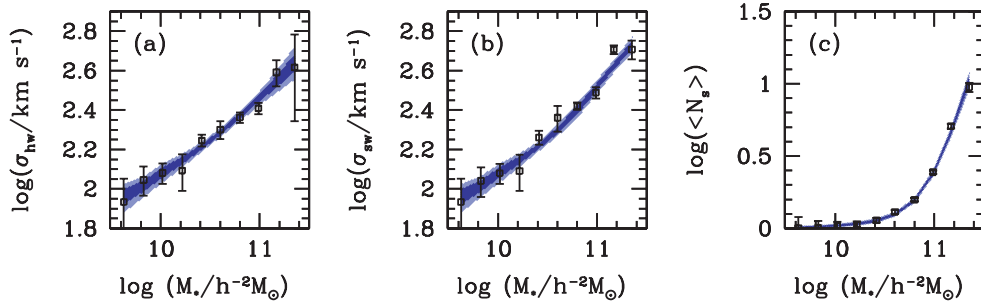
Figure 7. Same as Fig. 2, but as a function of the stellar mass of the centrals, based on sample SA. As for Fig. 2, these observables are not used to constrain the model parameters.

and 95 per cent confidence levels obtained from our MCMC. As in the case of the MLR, the model accurately fits the data, also in the case of sample SA, which is not used to constrain the model (see Fig. 7). The 16, 50 and 84 percentile values of our model parameters obtained from our analysis are listed in Table 3.

Fig. 8 is the same as Fig. 3, except that it shows the constraints on the MSR, rather than the MLR. At the massive end, the average stellar mass of red centrals scales with halo mass as $M_* \propto M^{0.33^{+0.12}_{-0.14}}$ while for blue centrals we find that $M_* \propto M^{0.99^{+0.32}_{-0.51}}$. For the scatter in $P(M_*|M)$ we obtain that $\sigma_{\log M_*} = 0.17^{+0.04}_{-0.03}$ for red centrals and $\sigma_{\log M_*} = 0.15^{+0.11}_{-0.08}$ for blue centrals. The posterior distribution of

$\sigma_{\log M_*}$ for blue centrals has a long tail extending to large values of scatter. At the low end, the confidence levels for $\sigma_{\log M_*}$ are largely dominated by our prior ($\sigma_{\log M_*} > 0.04$), which has been adopted for computational convenience. Hence, we cannot rule out that the data are consistent with zero scatter (i.e. $\sigma_{\log M_*} = 0.0$) for blue centrals stacked by stellar mass.

In Fig. 9 we present the average halo mass and the scatter in halo masses obtained from our analysis for red centrals (left-hand panels), blue centrals (middle panels) and all centrals (right-hand panels) as a function of stellar mass. Note that the scatter in halo masses increases with stellar mass for the red centrals, while it is

Table 3. MSR: percentiles of the posterior distribution.

	Parameter	16 per cent	50 per cent	84 per cent	Best fit
Red centrals	$\log(M_{*0})$	10.15	10.58	10.93	10.84
	$\log(M_1)$	11.46	11.94	12.30	12.18
	γ_1	2.41	3.39	4.48	3.34
	γ_2	0.19	0.33	0.45	0.22
	$\sigma_{\log M_*}$	0.14	0.17	0.21	0.15
Blue centrals	$\log(M_{*0})$	8.35	9.42	10.71	9.38
	$\log(M_1)$	10.56	11.29	11.99	11.32
	γ_1	2.30	3.19	4.36	2.41
	γ_2	0.48	0.99	1.31	1.12
	$\sigma_{\log M_*}$	0.07	0.15	0.26	0.12
All centrals	f_0	0.38	0.46	0.57	0.56
	α_f	0.44	0.62	0.78	0.46
	$\log N_{12}$	−0.91	−0.78	−0.68	−0.71
	α	1.15	1.24	1.34	1.17

The 16, 50 and 84 percentile values of the posterior distributions for the parameters and the best-fitting parameters of our model obtained from the MCMC analysis of the velocity dispersion data from Samples SR, SB and SA. The best-fitting model has a reduced $\chi^2 = 0.53$.

roughly independent of stellar mass for blue centrals. In the right-hand panel of Fig. 5 we compare the MSR of red centrals (triangles) to that of blue centrals (circles) and to that of all centrals (squares). At $M_* \lesssim 10^{10.5}\, h^{-2}\, \mathrm{M}_\odot$, the average halo mass of red centrals is virtually identical to that of blue centrals, certainly within the error bars. At larger stellar masses, red centrals reside on average in more massive haloes than blue centrals. In contrast, at fixed luminosity (see left-hand panel), the average halo mass of red centrals is *always* systematically larger that that of blue centrals, by more than a factor of 3. Hence, we conclude that stellar mass is a better indicator of halo mass than luminosity, especially at the low-mass end. However,

we also stress that there still is a significant amount of scatter in the relation between the stellar mass of a central galaxy and the mass of the halo in which it resides.

Finally, recall that we have assumed that the number of satellites in a given halo, $\langle N_s \rangle_M$, is independent of the colour of its central. In order to test the possible implications of this assumption, we have repeated the above analysis allowing for independent $\langle N_s \rangle_M$ for haloes with red and blue centrals (each parametrized with equation 21). This adds an additional two free parameters to the model, bringing the total to 16. We find that the resulting constraints are perfectly consistent with $\langle N_s \rangle_M$ being identical for red and blue centrals, and that all other constraints are similar to what we presented above. Hence, we conclude that our assumption that $\langle N_s \rangle_M$ is independent of the colour of its central is supported by the data and does not bias our results.

4.3 Comparison with other studies

It is interesting and important to compare our constraints on the MLR and MSR of central galaxies to those obtained using different, independent data sets and methods, including galaxy group catalogues, galaxy–galaxy lensing, galaxy clustering, halo abundance matching and other studies of satellite kinematics. In order to enable a fair and meaningful comparison, whenever required we have adapted the results in the literature to match the definitions of halo mass and stellar mass used in this paper. In particular, we follow Hu & Kravtsov (2003) to convert between different definitions of halo mass and use the results of Bell et al. (2003) and Borch et al. (2006) to convert stellar masses to the Kroupa (2001) initial mass function adopted here.

Yang et al. (2007) studied galaxy groups in the SDSS, to which they assigned halo masses based upon either the total stellar mass or the total luminosity content of each group. We use their group
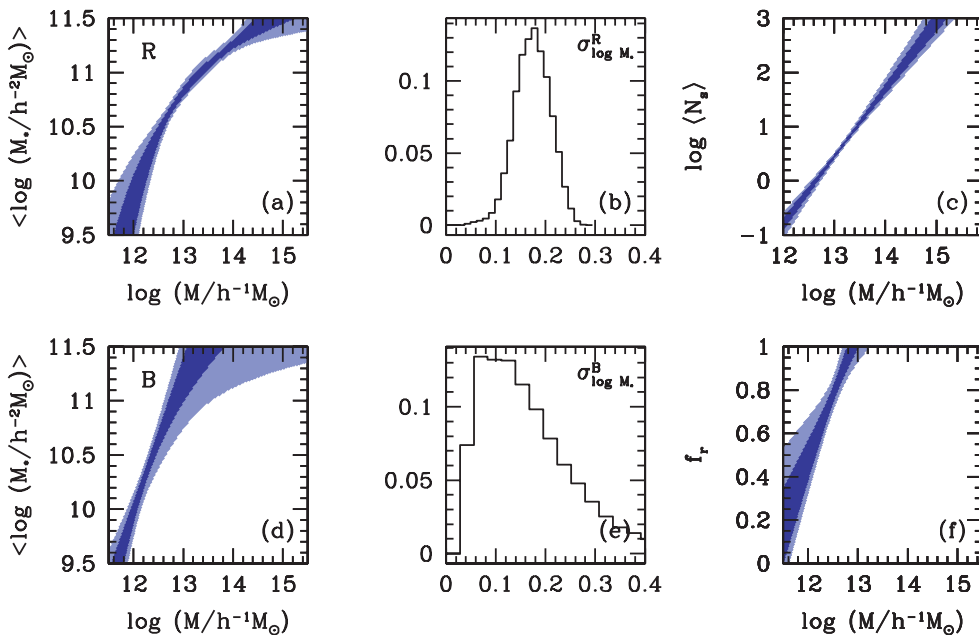
Figure 8. Constraints on the model ingredients obtained from the MCMC The 68 and 95 per cent confidence intervals are indicated as dark and faint blue regions, respectively. Panel (a) shows the average stellar mass of red centrals as a function of halo mass, while panel (b) shows the posterior distribution of the scatter $\sigma_{\log M_*}$ in this relation. Panels (d) and (e) show the same but for blue centrals. Panel (c) shows the constraints on the average number of satellites as a function of halo mass, and finally, panel (f) shows the constraints on the fraction of red centrals as a function of halo mass.
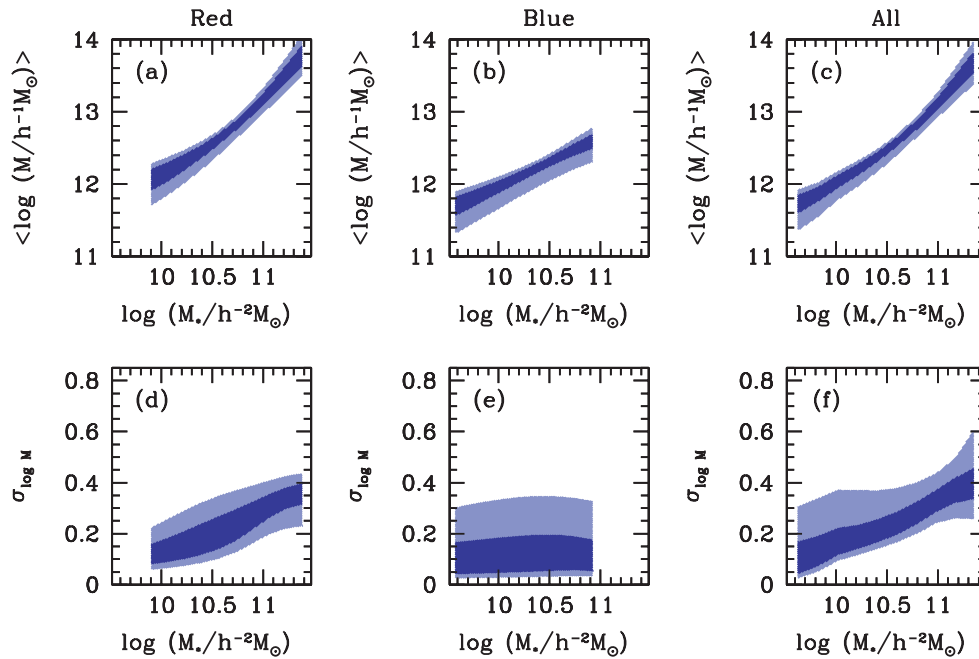
Figure 9. Same as Fig. 4, but for the MSR, rather than the MLR.

catalogue to investigate the MLR and MSR of central galaxies, with and without the split in red and blue by colour. The solid and dashed lines in Figs 10 and 11 correspond to the MLR and MSR of central galaxies in their group catalogue, where the halo masses have been assigned using the total stellar mass and total luminosity content of the groups, respectively.

Mandelbaum et al. (2006) measured the galaxy–galaxy lensing signal in the SDSS for galaxies stacked by luminosity and by stellar mass. The galaxies were split into early and late types based upon their morphology. Here we make the crude assumption that this is equivalent to our split in red and blue; although clearly an over-simplification, we do not believe that this invalidates a comparison with our results. Modelling their data, they obtained the MLR and MSR indicated in Figs 10 and 11 by open squares with error bars. The same exercise was repeated in Mandelbaum et al. (2008), but by stacking isolated galaxies. The results of this analysis are shown as filled squares with error bars (95 per cent) in Fig. 11. In the same figure, we also show the galaxy–galaxy lensing results of Schulz et al. (2009) as hexagons with error bars (95 per cent).

The abundance and clustering of galaxies hold important information regarding the halo occupation statistics of these galaxies. Using the observed luminosity function and clustering properties of galaxies in the SDSS, Cacciato et al. (2009) constrained the conditional luminosity function, $\Phi(L|M)$, which describes the average number of galaxies of luminosity L that reside in a halo of mass M (Yang et al. 2003). We use their best-fitting parameters to calculate the MLR of central galaxies and show it using open circles[5] in the top left-hand panel of Fig. 10. Note that Cacciato et al. (2009) have also shown that their halo occupation model is able to reproduce the galaxy–galaxy lensing signal obtained by stacking central galaxies based upon their luminosities.

The relation between galaxy stellar mass and halo mass can also be obtained by matching the abundance of galaxies to the abundance of haloes and subhaloes that host these galaxies (e.g. Conroy, Wechsler & Kravtsov 2006; Shankar et al. 2006; Conroy et al. 2009; Guo et al. 2010; Moster et al. 2010; Behroozi et al. 2010). The results from this (sub)halo abundance matching technique are often quoted as the mean of the distributions $P(\log M_*|M)$. We asked the respective authors to provide us $\log\langle M\rangle(M_*)$ to enable a fair comparison. In the top left panel of Fig. 11 we show the results of Moster et al. (2010, dotted line), Guo et al. (2010, dot–long-dashed line) and Behroozi et al. (2010, dot–dashed line).

Finally, using data from the SDSS and the DEEP2 survey, Conroy et al. (2007) used the kinematics of satellite galaxies to determine the evolution of the stellar mass-to-light ratio of central galaxies from $z \sim 1$ to $z \sim 0$. They measured and modelled the radial dependence of the velocity dispersion (in contrast to the aperture averaged velocity dispersions used in this paper) to infer the average halo mass as a function of the stellar mass of the central galaxy. The halo mass–stellar mass relation for all central galaxies thus obtained from their analysis at $z \sim 0$ is shown in Fig. 11 using circles with error bars.

In all panels of Figs 10 and 11, the shaded areas show the 95 per cent confidence intervals obtained in this paper using the kinematics of satellite galaxies. Overall, the results obtained using all these very different methods are in remarkably good agreement with each other (see also Behroozi et al. 2010; Dutton et al. 2010), and with the results obtained here. However, there also are a few discrepancies, which we discuss below.

With regard to the MLR, the galaxy group catalogues of Yang et al. (2007) and the galaxy–galaxy lensing analysis of Mandelbaum et al. (2006) yield halo masses around red centrals that are in good agreement with each other. But at $L \sim 10^{10}\,h^{-2}\,\mathrm{L}_\odot$, the halo masses inferred from these two methods are roughly a factor 2 lower compared to the results obtained here. The three methods,

---

[5] Cacciato et al. (2009) also used results from the group catalogue of Yang et al. (2007) to constrain their model, which explains why (i) their error bars are extremely small and (ii) their results are in perfect agreement with those of Yang et al. (2007).
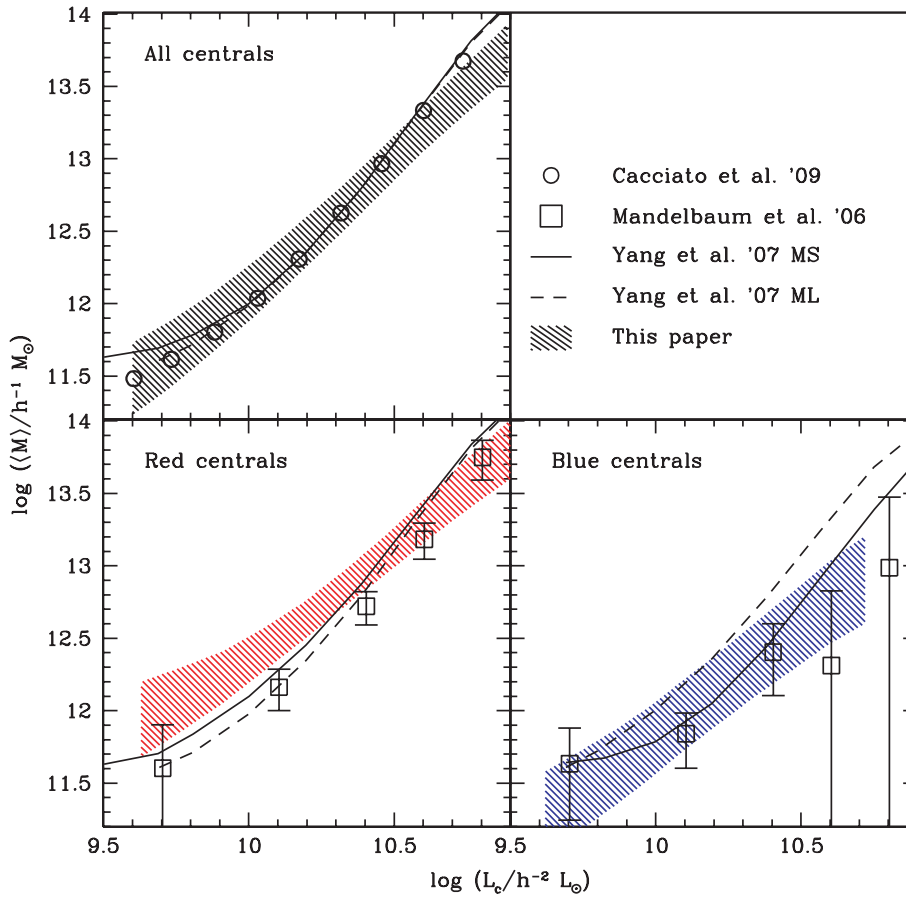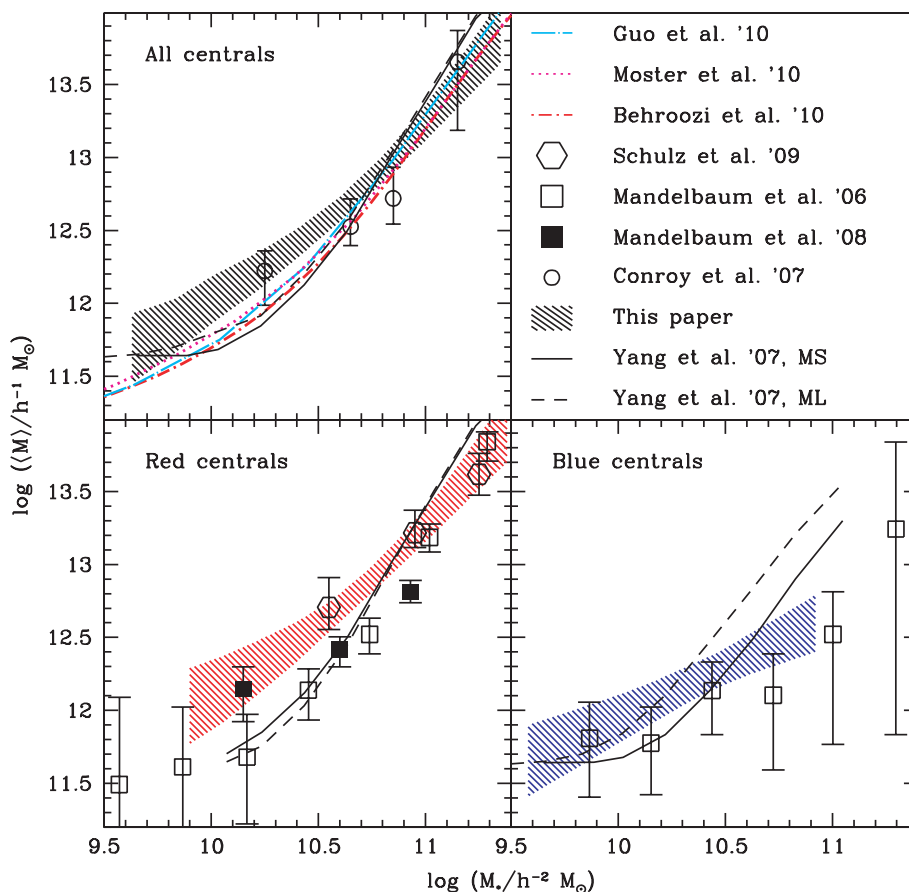
Figure 10. Comparison of our MLR constraints with other constraints from the literature. The shaded regions show the 95 per cent confidence intervals that we obtained from the analysis of satellite kinematics. The circles show the MLR obtained by Cacciato et al. (2009) by using galaxy abundance and clustering measurements (the corresponding 95 per cent confident intervals are smaller than the circles), the squares with error bars (95 per cent confidence intervals) show the MLR obtained by Mandelbaum et al. (2006) using weak lensing. The solid and dashed lines show the MLR obtained from the group catalogue of Yang et al. (2007).

however, agree fairly well at the bright end. Somewhat surprisingly, the MLR of all centrals (upper left-hand panel of Fig. 10) does not reveal any discrepancy between the masses inferred from satellite kinematics, versus those inferred from either clustering (results of Cacciato et al. 2009) or galaxy group catalogues (results of Yang et al. 2007). In case of the MSR of red centrals, at the low stellar mass end the group catalogue results agree with the weak lensing results and are again a factor 2–3 lower than the results obtained here. On the other hand, at the bright end, our results agree fairly well with the weak lensing results while the group catalogue results are roughly larger by a factor of 1.6. It is also worth noting that the weak lensing results are not fully consistent with each other at the intermediate and low-mass ends. In particular, our results are in excellent agreement with the weak lensing analysis of Schulz et al. (2009) and the low-mass point of Mandelbaum et al. (2008). For the MSR of all centrals (upper left-hand panel of Fig. 11), our analysis of satellite kinematics once again yields halo masses around low-mass centrals that are ∼0.3 dex larger than those inferred using either subhalo abundance matching or galaxy group catalogues. It is noteworthy, though, that the results obtained by Conroy et al. (2007), which are also based on satellite kinematics, are actually in good agreement with our results. Finally, we note that for blue centrals there is no clear indication of any systematic discrepancy, except perhaps at the massive end. However, since the massive (bright) end of the galaxy mass (luminosity) function is

dominated by red centrals, the corresponding number statistics are poor resulting in large error bars. Consequently, we do not consider this discrepancy significant.

To summarize, Figs 10 and 11 indicate that tremendous progress has been made in recent years in constraining the galaxy–dark matter connection, with different techniques yielding MLRs and MSRs that are in fairly good agreement with each other, typically within a factor of 2. While it is difficult to make any robust statement about possible systematics, we acknowledge that there is a hint that satellite kinematics yields halo masses around low-mass centrals that are systematically larger than most other methods, especially around red centrals. Although we certainly can't rule out any systematics in the other methods, we briefly discuss a potential problem with satellite kinematics.

Recently, Skibba et al. (2010) analyzed the SDSS galaxy group catalogue of Yang et al. (2007) and showed that in a significant fraction of groups (ranging from ∼25 per cent at the low-mass end to ∼40 per cent at the massive end) the brightest group member is a satellite galaxy rather than a central. As discussed at length in their paper, this could cause satellite kinematics to overestimate halo masses by as much as a factor of ∼1.6. However, we consider it unlikely that this explains the systematic offset between satellite kinematics and other methods because of the following two reasons. First of all, the effect is expected to be largest at the massive end, and to be negligible at the low-mass end, opposite to the trends seen in

Figure 11. Comparison of our MSR constraints with other constraints from the literature. The shaded regions show the 95 per cent confidence intervals that we obtained from the analysis of satellite kinematics. The circles with error bars (68 per cent confidence intervals) show the MSR obtained by Conroy et al. (2007) using satellite kinematics. The open squares, the solid squares and the hexagons with error bars (95 per cent confidence intervals) show the MSR obtained by Mandelbaum et al. (2006), Mandelbaum et al. (2008) and Schulz et al. (2009), respectively, using weak lensing. The solid and dashed lines show the MSR obtained from the group catalogue of Yang et al. (2007). The (magenta) dotted line, the (red) dot–dashed line and the (cyan) dot–long-dashed line show the results from abundance matching studies from Moster et al. (2010), Behroozi, Conroy & Wechsler (2010) and Guo et al. (2010), respectively.

Figs 10 and 11. Secondly, the factor $\sim$1.6 overestimate only occurs if the probability $\mathcal{P}_{\mathrm{BNC}}(M)$ that the brightest (most massive) galaxy in a halo of mass M is not the central galaxy is independent of the luminosity (stellar mass) of the central galaxy. However, if haloes of mass M in which the central galaxy is fainter (less massive) than the average for haloes of that mass are more prone to having a brighter (more massive) satellite, which does not seem unreasonable, then the effect can be much weaker (see Skibba et al. 2010, for details).

To investigate the possibility that our results for red centrals at the low stellar mass end are affected by haloes in which the central galaxy is not the most massive, we perform the following test. We take all hosts from Sample SR that have stellar masses in a bin of width 0.17 dex centred around $\log{(M_*/h^{-2}\,M_\odot)} = 10.39$. For each host, we determine the ratio, $\mathcal{R}_{12}$, of its stellar mass to that of its most massive satellite. Under the assumption that a larger $\mathcal{R}_{12}$ implies a larger probability that this host is a true central, we proceed as follows. We sort the hosts in decreasing order of $\mathcal{R}_{12}$, and create five samples by discarding the final 10, 20, 30, 40 and 50 per cent of the hosts (plus their satellites), respectively. For each of these samples we compute the satellite-weighted velocity dispersion of the remaining satellites, which we plot in Fig. 12 as a function of the minimum value of $\mathcal{R}_{12}$. Clearly, within the error bars there is no indication for a systematic trend between σ_{sw} and $\mathcal{R}_{12}^{\mathrm{min}}$. Although
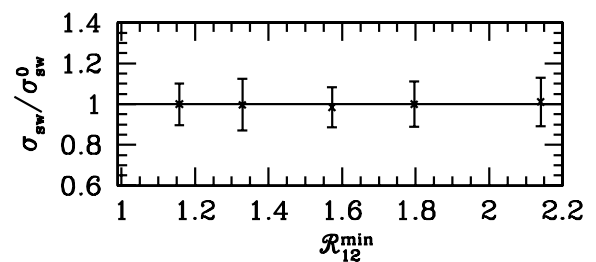
Figure 12. The ratio of the satellite-weighted velocity dispersion, σ_{sw}, measured around hosts that have $\mathcal{R}_{12}$ (the ratio of their own stellar mass to that of their most massive satellite) greater than or equal to $\mathcal{R}_{12}^{\mathrm{min}}$, to the ratio of the satellite-weighted velocity dispersion measured around all hosts (σ_{sw}^0).

this does not rule out that our satellite kinematics are affected by the possibility that a certain fraction of our host galaxies in reality are satellites rather than centrals, it certainly makes it less likely.

5 SUMMARY

We have used the kinematics of satellite galaxies in order to probe the halo mass–luminosity relation (MLR) and the halo mass–stellar mass relation (MSR) of central galaxies. For this purpose, an

iterative selection criterion was first applied to select central and satellite galaxies from a volume-limited subsample of the SDSS. The resulting sample consist of ~6000 satellites around ~3700 centrals, making it the largest volume-limited sample of central-satellite pairs used to date for studies of satellite kinematics. Since the number of satellite galaxies around any individual central galaxy is small, a stacking procedure was used to combine the velocity information of the satellite galaxies of centrals with similar luminosities or stellar masses. A detailed modelling procedure, outlined in Paper I, was then used to infer both the average scaling relation between halo mass and the central galaxy property and its scatter.

As expected, and in qualitative agreement with many other studies, we find that more luminous (more massive) centrals reside in more massive haloes. In addition, we find that the MLR of central galaxies is different for central galaxies of different colour: red centrals, on average, occupy more massive haloes than blue centrals of the same luminosity. Consequently, the scatter in the MLR of central galaxies is at least partly correlated with the colour of the central galaxy.

When stacking central galaxies according to their stellar masses, we find the difference in the mean MSRs of red and blue centrals to be less pronounced than in the case of the MLR. In particular, for $M_* \lesssim 10^{10.5} \, h^{-2} \, \mathrm{M_\odot}$, the average halo masses of red and blue centrals are not significantly different. We thus conclude that the stellar mass of a central galaxy is a more reliable indicator of its halo mass than its (r-band) luminosity. However, even the MSR has a significant amount of scatter of the order of ~0.2 dex in stellar mass at fixed halo mass. This translates into a scatter in halo mass at fixed stellar mass that increases from ~0.1 dex at $M_* \simeq 4 \times 10^9 \, h^{-2} \, \mathrm{M_\odot}$ to ~0.4 dex at $M_* \simeq 2 \times 10^{11} \, h^{-2} \, \mathrm{M_\odot}$.

We compared our constraints on the MLR and MSR of central galaxies with a number of other, independent constraints coming from the SDSS galaxy group catalogue of Yang et al. (2007); the galaxy–galaxy lensing analyses of Mandelbaum et al. (2006), Mandelbaum et al. (2008) and Schulz et al. (2009); the galaxy clustering analysis of Cacciato et al. (2009); subhalo abundance matching studies of Moster et al. (2010), Guo et al. (2010) and Behroozi et al. (2010); and the analysis of satellite kinematics by Conroy et al. (2007). Overall, there is good agreement among all these different studies, with a typical study-to-study scatter of less than a factor 2, which is comparable to the typical 2σ errors quoted by most of these studies. There is some indication, though, that satellite kinematics yield halo masses around low-mass centrals ($M_* \lesssim 3 \times 10^{10} \, h^{-2} \, \mathrm{M_\odot}$) that are systematically higher by a factor of 2–3 that most other methods, although we emphasize that our results are in perfect agreement with the galaxy–galaxy lensing analysis of Schulz et al. (2009). As discussed in the text, we do not believe that our results are significantly affected by the fact that not all central galaxies are the brightest (or most massive) galaxies in their dark matter haloes, as shown by Skibba et al. (2010). In fact, detailed tests with mock galaxy redshift surveys, presented in Paper II, have revealed no systematic effects for our method of analysis.

We conclude that the overall level of agreement regarding the MLR and MSR among all different techniques indicates that we are converging on an accurate and reliable description of the galaxy–dark matter connection (see also van den Bosch et al. 2007; Behroozi et al. 2010; Dutton et al. 2010). In addition to an overall agreement regarding the means of the MSR and MLR, to well within a factor of 2, there is also good agreement regarding the amount of scatter; as demonstrated in Paper II, the scatter of ~0.2 dex in luminosity or stellar mass at fixed halo mass is in excellent agreement with independent constraints obtained by Yang et al. (2008), Cacciato

et al. (2009) and Cooray (2006), and with predictions from the semi-analytical model for galaxy formation of Croton et al. (2006). This overall level of agreement is an admirable achievement, which will prove invaluable not only for furthering our understanding of galaxy formation, but also for using galaxies to probe the cosmic density field and to constrain cosmological parameters.

REFERENCES

Adelman-McCarthy J. K. et al., 2006, ApJS, 162, 38
Baldry I. K., Glazebrook K., Brinkmann J., Ivezić Ž, Lupton R. H., Nichol R. C., Szalay A. S., 2004, ApJ, 600, 681
Becker M. R. et al., 2007, ApJ, 669, 905
Behroozi P. S., Conroy C., Wechsler R. H., 2010, ApJ, 717, 379
Bell E. F., McIntosh D. H., Katz N., Weinberg M. D., 2003, ApJS, 149, 289
Blanton M. R. et al., 2003a, ApJ, 592, 819
Blanton M. R. et al., 2003b, AJ, 125, 2348
Blanton M. R. et al., 2005, AJ, 129, 2562
Borch A. et al., 2006, A&A, 453, 869
Brainerd T. G., Specian M. A., 2003, ApJ, 593, L7
Brown M. J. I. et al., 2008, ApJ, 682, 937
Cacciato M., van den Bosch F. C., More S., Li R., Mo H. J., Yang X., 2009, MNRAS, 394, 929
Carlberg R. G., Yee H. K. C., Ellingson E., Abraham R., Gravel P., Morris S., Pritchet C. J., 1996, ApJ, 462, 32
Carlberg R. G., Yee H. K. C., Ellingson E., 1997, ApJ, 478, 462
Collister A. A., Lahav O., 2005, MNRAS, 361, 415
Conroy C., Wechsler R. H., 2009, ApJ, 696, 620
Conroy C. et al., 2005, ApJ, 635, 982
Conroy C., Wechsler R. H., Kravtsov A. V., 2006, ApJ, 647, 201
Conroy C. et al., 2007, ApJ, 654, 153
Cooray A., 2006, MNRAS, 365, 842
Croton D. J. et al., 2006, MNRAS, 365, 11
Dai X., Kochanek C. S., Morgan N. D., 2007, ApJ, 658, 917
Dutton A. A., Conroy C., van den Bosch F. C., Prada F., More S., 2010, MNRAS, 407, 2
Erickson L. K., Gottesman S. T., Hunter J. H., Jr, 1987, Nat, 325, 779
Gavazzi R., Treu T., Rhodes J. D., Koopmans L. V. E., Bolton A. S., Burles S., Massey R. J., Moustakas L. A., 2007, ApJ, 667, 176
Guo Q., White S., Li C., Boylan-Kolchin M., 2010, MNRAS, 404, 1111
Hu W., Kravtsov A. V., 2003, ApJ, 584, 702
Komatsu E. et al., 2010, preprint (arXiv:1001.4538)
Kravtsov A. V., Berlind A. A., Wechsler R. H., Klypin A. A., Gottlöber S., Allgood B., Primack J. R., 2004, ApJ, 609, 35
Kroupa P., 2001, MNRAS, 322, 231
Li R., Mo H. J., Fan Z., Cacciato M., van den Bosch F. C., Yang X., More S., 2009, MNRAS, 394, 1016
Macciò A. V., Dutton A. A., van den Bosch F. C., Moore B., Potter D., Stadel J., 2007, MNRAS, 378, 55
McKay T. A. et al., 2001, preprint (astro-ph/0108013)
McKay T. A. et al., 2002, ApJ, 571, L85
Mandelbaum R., Seljak U., Kauffmann G., Hirata C. M., Brinkmann J., 2006, MNRAS, 368, 715
Mandelbaum R., Seljak U., Hirata C. M., 2008, J. Cosmol. Astropart. Phys., 8, 6

More S., 2009, PhD thesis, Ruprechts-Karls-Universität, Heidelberg

More S., van den Bosch F. C., Cacciato M., Mo H. J., Yang X., Li R., 2009a, MNRAS, 392, 801 (Paper II)

More S., van den Bosch F. C., Cacciato M., 2009b, MNRAS, 392, 917 (Paper I)

Moster B. P., Somerville R. S., Maulbetsch C., van den Bosch F. C., Maccio' A. V., Naab T., Oser L., 2010, ApJ, 710, 903

Navarro J. F., Frenk C. S., White S. D. M., 1997, ApJ, 490, 493

Norberg P., Frenk C. S., Cole S., 2008, MNRAS, 383, 646

Parker L. C., Hoekstra H., Hudson M. J., van Waerbeke L., Mellier Y., 2007, ApJ, 669, 21

Prada F. et al., 2003, ApJ, 598, 260

Rubin V. C., Ford W. K., Jr, Thonnard N., Burstein D., 1982, ApJ, 261, 439

Rykoff E. S. et al., 2008, ApJ, 675, 1106

Schulz A. E., Mandelbaum R., Padmanabhan N., 2009, preprint (arXiv:0911.2260)

Seljak U., 2000, MNRAS, 318, 203

Shankar F., Lapi A., Salucci P., De Zotti G., Danese L., 2006, ApJ, 643, 14

Skibba R., Sheth R. K., Connolly A. J., Scranton R., 2006, MNRAS, 369, 68

Skibba R. A., Sheth R. K., 2009, MNRAS, 392, 1080

Skibba R. A., van den Bosch F. C., Yang X., More S., Mo H., Fontanot F., 2010, MNRAS, in press (arXiv:1001.4533)

Tinker J. L., Weinberg D. H., Zheng Z., Zehavi I., 2005, ApJ, 631, 41

Tinker J., Kravtsov A. V., Klypin A., Abazajian K., Warren M., Yepes G., Gottlöber S., Holz D. E., 2008, ApJ, 688, 709

van den Bosch F. C., Yang X., Mo H. J., 2003, MNRAS, 340, 771

van den Bosch F. C., Norberg P., Mo H. J., Yang X., 2004, MNRAS, 352, 1302

van den Bosch F. C. et al., 2007, MNRAS, 376, 841

van den Bosch F. C., Aquino D., Yang X., Mo H. J., Pasquali A., McIntosh D. H., Weinmann S. M., Kang X., 2008, MNRAS, 387, 79

Yang X., Mo H. J., van den Bosch F. C., 2003, MNRAS, 339, 1057

Yang X., Mo H. J., van den Bosch F. C., Weinmann S. M., Li C., Jing Y. P., 2005, MNRAS, 362, 711

Yang X., Mo H. J., van den Bosch F. C., Pasquali A., Li C., Barden M., 2007, ApJ, 671, 153

Yang X., Mo H. J., van den Bosch F. C., 2008, ApJ, 676, 248

Yang X., Mo H. J., van den Bosch F. C., 2009, ApJ, 695, 900

Yoo J., Tinker J. L., Weinberg D. H., Zheng Z., Katz N., Davé R., 2006, ApJ, 652, 26

York D. G. et al., 2000, AJ, 120, 1579

Zaritsky D., White S. D. M., 1994, ApJ, 435, 599

Zaritsky D., Smith R., Frenk C., White S. D. M., 1993, ApJ, 405, 464

Zaritsky D., Smith R., Frenk C., White S. D. M., 1997, ApJ, 478, 39

Zehavi I. et al., 2004, ApJ, 608, 16

Zehavi I. et al., 2005, ApJ, 630, 1

Zheng Z., Coil A. L., Zehavi I., 2007, ApJ, 667, 760

APPENDIX A: SAMPLE SELECTION FUNCTION

Here we illustrate how our use of a volume-limited sample of galaxies, complete in luminosity, leads to a sample that is incomplete in stellar mass. Our aim is to characterize the sample selection function, $S(M_*, C)$, which describes the fraction of galaxies of stellar mass M_* and colour C that make it into our sample. This sample selection function is required for modelling the satellite kinematics as a function of the stellar mass of their host galaxy (see Section 3.3.2)

The left-hand panel of Fig. A1 shows the distribution of galaxies in the $^{0.1}r$-band luminosity–redshift plane. Red and blue galaxies are indicated by red and blue dots, respectively. The apparent magnitude limit, $m_r^{\mathrm{lim}} = 17.77$, of the spectroscopic sample results in an absolute magnitude limit given by

$$^{0.1}M_r^{\mathrm{lim}} - 5\log h = 17.77 - \mathrm{DM}(z) - k_{0.1}(z)$$
$$+ 1.62\,(z - 0.1)\,. \qquad (A1)$$

Here $k_{0.1}(z)$ is the k-correction to redshift $z = 0.1$, 1.62 is the evolution correction factor from Blanton et al. (2003a) and $\mathrm{DM}(z)$ is given by

$$\mathrm{DM}(z) = 5\log D_{\mathrm{L}}(z) + 25.0\,, \qquad (A2)$$

where $D_{\mathrm{L}}(z)$ is the luminosity distance of the galaxy in $h^{-1}\,\mathrm{Mpc}$. The redshift dependence of the k-corrections is fairly well reproduced by (van den Bosch et al. 2008)

$$k_{0.1}(z) = 2.5\log\left(\frac{z + 0.9}{1.1}\right)\,. \qquad (A3)$$

The above equations yield the solid black line in the left-hand panel of Fig. A1. Note that a very small fraction of galaxies fall below this predicted limit. This is because the k-correction also depends on the colour of the central galaxy which we have not accounted
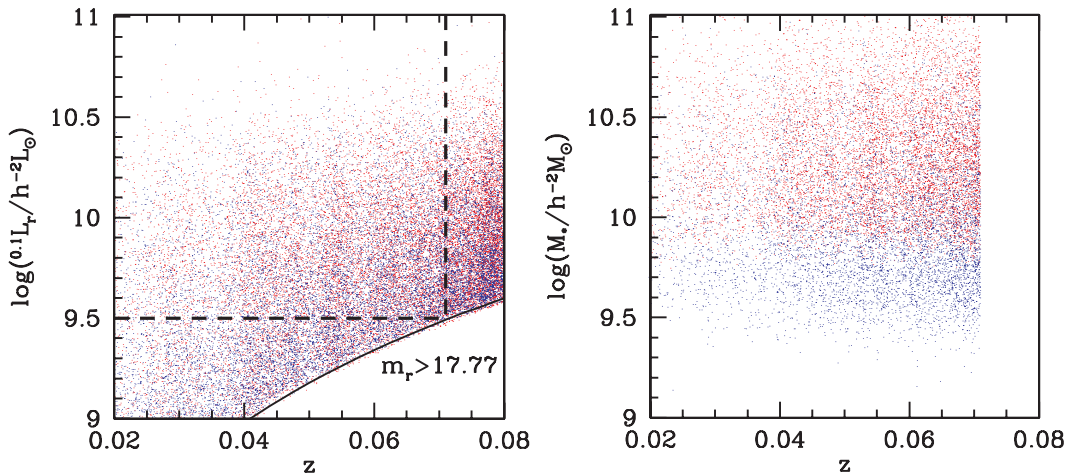
Figure A1. The left panel shows the distribution of SDSS galaxies in the luminosity-redshift plane. Red and blue galaxies are indicated by red and blue dots, respectively. The volume-limited sample of galaxies used for our analysis of satellite kinematics is enclosed by the dashed lines. The right-hand panel shows the distribution of galaxies in this volume-limited sample in the stellar mass-redshift plane.

for. However, this effect can safely be ignored for the purpose of this paper.

Galaxies with $z \leq 0.071$ and $^{0.1}L_r \geq 10^{9.5}$ (i.e. $^{0.1}M_r^{\mathrm{lim}} - 5\log h \leq -18.99$) make up the volume-limited sample used in this paper (indicated by dashed lines in the left-hand panel of Fig. A1). The right-hand panel of Fig. A1 shows the distribution of galaxies in this volume-limited sample in the stellar mass–redshift plane. Note that the sharp cut in luminosity translates into a colour-dependent cut in stellar mass; bluer galaxies have a lower cut-off in stellar mass, causing the low-mass end of the sample to be completely dominated by blue galaxies.

We remind the reader that in our analysis, galaxies were assigned stellar masses using the $^{0.0}(g - r)$ colour and the $^{0.0}r$-band magnitude using equation (1). The $^{0.1}r$-band magnitude limit we have used for our volume-limited sample translates into a $^{0.0}r$-band limit given by

$$^{0.0}M_r^{\mathrm{lim}} = {}^{0.1}M_r^{\mathrm{lim}} + [k_{0.1}(z) - k_{0.0}(z)] - 0.162, \tag{A4}$$

where the term in square brackets is the difference in k-corrections between redshift 0.0 and 0.1, and the last term is the difference in the evolution corrections between these redshifts. The k-corrections to redshift 0.0 can be reasonably well described by (van den Bosch et al. 2008)

$$k_{0.0}(z) = 2.5 \log(1 + z) + 1.5 z \, [^{0.0}(g - r) - 0.66]. \tag{A5}$$

Combining equations (A4), (A5), (A3) with equation (1) gives that, at fixed $^{0.0}(g - r)$ colour, the stellar mass limit in the volume-limited sample varies with $^{0.0}(g - r)$ and redshift as

$$\log(M_*^{\mathrm{lim}}) = 8.9812 - \log\left[\frac{z + 0.9}{1.1\,(1 + z)}\right]$$
$$- 0.396\,z + (1.097 + 0.6\,z)\,^{0.0}(g - r). \tag{A6}$$

In Fig. A2, we plot the distribution of galaxies in the colour–stellar mass diagram. The colour cut which was used to assign colours to our sample of galaxies is shown by the black solid line (see equation 1). The green dashed line show the limit expressed in equation (A6) assuming $z = 0.071$. At fixed stellar mass, only a fraction of galaxies (those that lie below the green line) are part of the volume-limited sample. More than half of the red galaxies drop out of the sample at stellar masses below $10^{9.8}\,h^{-2}\,\mathrm{M}_\odot$.
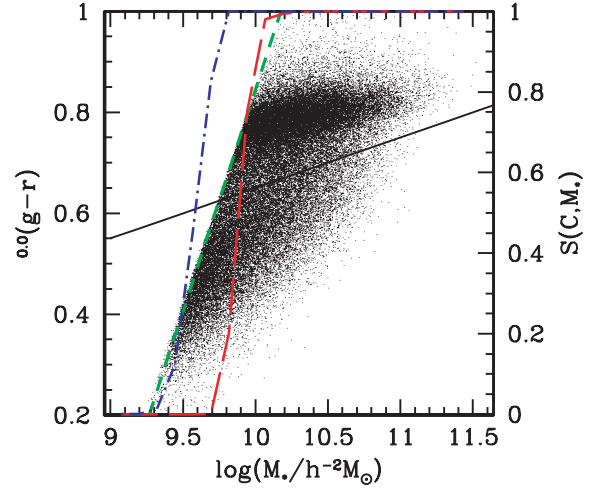
Figure A2. The colour–stellar mass diagram of galaxies in our volume-limited sample. The black solid line shows the boundary that we use to split the galaxy population in 'red' and 'blue' galaxies. The green dashed line shows the analytical prediction (equation A6) for the selection effect that results due to our use of a volume-limited sample complete in luminosity. The resulting selection functions, $S(C, M_*)$, for red and blue galaxies are indicated by the (red) dashed and (blue) dot–dashed lines, respectively.

To calculate the selection function $S(M_*, C)$, we use the entire flux limited catalogue of galaxies to populate the $^{0.0}(g - r)$–stellar mass plane, this time assigning to each galaxy a weight equal to 1 over the maximum volume to which this galaxy could be seen given the r-band flux limit of 17.77. Using small bins in stellar mass, we calculate $S(M_*, C)$ in each bin by dividing the sum of weights of galaxies of a particular colour that lie below $\log(M_*^{\mathrm{lim}})$ with the sum of weights of all galaxies of that colour in the bin under consideration. The resulting selection functions for red and blue galaxies are plotted in Fig. A2 as red long-dashed and blue dot–dashed lines, respectively.

This paper has been typeset from a TEX/LATEX file prepared by the author.